Plasma Physics and
Controlled Fusion

Centrifugal-mirror confinement with strong azimuthal magnetic field

To cite this article before publication: Timothy Stoltzfus-Dueck *et al* 2025 *Plasma Phys. Control. Fusion* in press https://doi.org/10.1088/1361-6587/adfe8e

Centrifugal-mirror confinement with strong azimuthal magnetic field

T. Stoltzfus-Dueck[1] and F. I. Parra[1]

[1]Princeton Plasma Physics Laboratory, Princeton, NJ 08540

E-mail: tstoltzf@pppl.gov

Abstract. One practical challenge for the centrifugal-mirror confinement concept is the large radial voltage necessary to drive supersonic azimuthal rotation. In principle, the addition of a strong azimuthal field could reduce the required voltage, since the simple azimuthal ExB drift would be replaced by more rapid azimuthal trapped-particle precession. Also, if the mirror ratio is large enough, newly ionized ions are accelerated to the necessary parallel velocities in their first bounce orbit, both confining and significantly heating them. Unfortunately, MHD analysis shows that the centrifugal-force-confining plasma current is purely azimuthal. This implies that only the axial magnetic field contributes to the confining magnetic pressure, severely limiting the usefulness of the azimuthal magnetic field in a beta-limited plasma scenario.

Keywords: centrifugal mirror, trapped-particle precession, MHD equilibrium, Grad-Shafranov Submitted to: *Plasma Phys. Control. Fusion*

1. Introduction

Centrifugal confinement systems have long been known to offer some significant potential advantages as a fusion device [1–3]. They do not require a plasma current to generate the confining magnetic field, thus avoiding the risk of disruptions due to current-driven instabilities. They can retain the geometrical simplicity of magnetic mirrors, while using supersonic rotation to close the loss cone and confine essentially all ions in the parallel direction [4, 5]. Further, both theoretical [6, 7] and experimental [8] investigations have suggested that their strong $\boldsymbol{E}\times\boldsymbol{B}$ shear effectively stabilizes MHD instabilities, so they might achieve confinement so good that it is limited by classical transport [4]. In addition, the radial electric field results in immediate heating of newly-ionized ions, via the polarization shift as they accelerate azimuthally to the $\boldsymbol{E}\times\boldsymbol{B}$ speed [9].

One technical challenge for this approach is the large electric potential difference that must be applied to maintain the strong azimuthal $\boldsymbol{E}\times\boldsymbol{B}$ rotation. As a simple estimate, equate the bulk azimuthal rotation $u_\varphi = M_\mathrm{i} v_\mathrm{ti}$ with the $\boldsymbol{E}\times\boldsymbol{B}$ speed $v_E = |\boldsymbol{v}_E|$ for $\boldsymbol{v}_E = \boldsymbol{E}\times\boldsymbol{B}/B^2$, with ion thermal speed $v_\mathrm{ti} \doteq (T_\mathrm{i}/m_\mathrm{i})^{1/2}$ and Mach number $M_\mathrm{i} \doteq u_\varphi/v_\mathrm{ti}$. The necessary potential ϕ can be estimated as $Z_\mathrm{i}e\phi/T_\mathrm{i} \sim M_\mathrm{i}(R_0/\rho_\mathrm{i})$ for characteristic device radius R_0 and ion gyroradius $\rho_\mathrm{i} \doteq v_\mathrm{ti}/\Omega_\mathrm{i}$, gyrofrequency $\Omega_\mathrm{i} \doteq Z_\mathrm{i}eB/m_\mathrm{i}$, and charge state Z_i. [For example parameters, see Appendix A.1.] As a further constraint, the magnetic field must be strong enough to confine the plasma in the radial direction, which leads to a limit $u_\varphi \lesssim v_\mathrm{A}$ for Alfvén speed $v_\mathrm{A} = B/\sqrt{\mu_0\rho_\mathrm{m}}$ with plasma mass density ρ_m, observed to be a hard limit in experiment [10]. Taken together, these imply the requirement $Z_\mathrm{i}e\phi/T_\mathrm{i} \gtrsim M_\mathrm{i}^2(R_0/\lambda_\mathrm{i})$ for $\lambda_\mathrm{i} = m_\mathrm{i}/(Z_\mathrm{i}e\sqrt{\mu_0\rho_\mathrm{m}})$ the ion skin depth. For a practical fusion reactor, it would clearly be desirable to ease these requirements for the applied voltage. To do this, we need to find a way to maintain the centrifugally-confining azimuthal velocity u_φ while reducing the electric field strength E.

One possible approach could be the addition of an azimuthal magnetic field. In contrast to previous applications, in which a weak azimuthal field was used to introduce stabilizing magnetic shear [3, 11], here we propose an azimuthal field that is significantly stronger than the axial field. Why would we do this? To see, let's adopt a simple cylindrical coordinate system

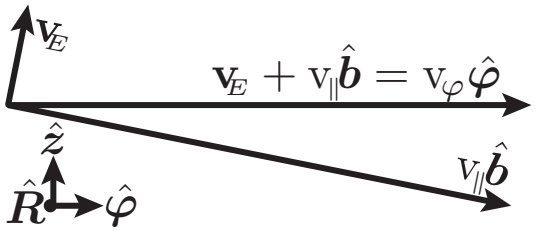

Figure 1. For axially trapped particles, the z components of $\boldsymbol{v}_E$ and $v_\parallel\hat{\boldsymbol{b}}$ must cancel, in the average. When the magnetic field is mostly azimuthal, this leads to an azimuthal rotation that is much larger than v_E itself.

R, φ, z, with $\hat{\boldsymbol{R}}\times\hat{\boldsymbol{\varphi}} = \hat{\boldsymbol{z}}$ for $\hat{\boldsymbol{z}}$ aligned with the trap's axis of symmetry, then consider the sketch in Fig. 1. In the average, an axially trapped particle must obviously have a vanishing velocity in the $\hat{\boldsymbol{z}}$ (axial) direction, i.e $\hat{\boldsymbol{z}}\cdot(v_\parallel\hat{\boldsymbol{b}} + \boldsymbol{v}_E) = 0$ with parallel velocity $v_\parallel$ and magnetic direction $\hat{\boldsymbol{b}}$. The azimuthal components of $v_\parallel\hat{\boldsymbol{b}}$ and $\boldsymbol{v}_E$ then turn out to be additive. If the magnetic field is mostly azimuthal, then $v_\parallel$ is quite a bit larger than v_E, leading to a much larger azimuthal rotation for a given electric field, as desired (Sec. 2.2). In addition, we will find that newly ionized ions would still be confined and significantly heated in their first bounce orbit, assuming one does not make the axial field too small (Sec. 2.3). Further, since the azimuthal magnetic field only varies as $1/R$, while the axial field strength goes as $1/R^2$ (along a flux surface), one could more easily achieve a large ratio of the confinement-region radius over the endcap radius, which enhances centrifugal confinement (Sec. 2.2).

Unfortunately, as we will show in Sec. 3, the equilibrium plasma current in this configuration would also be aligned purely azimuthally. Effectively, this implies that only the axial magnetic field contributes to the magnetic pressure that confines the plasma radially against the centrifugal force. Because of this, an azimuthal field may reduce the ion gyroradius in this configuration, but it will be unable to increase the allowable plasma pressure in a beta-limited case, severely restricting the set of scenarios in which an azimuthal field could be used to reduce the voltage required for centrifugal confinement.

We will derive the single-particle behavior in Sec. 2 and the MHD equilibrium properties in Sec. 3, then review our conclusions in Sec. 4. For reference, some frequently used symbols are identified in Table. 1.

Symbol	Definition
$\rho_{\varphi,z}$	gyroradius, with v_φ and B_z (Sec. 2.1).
ω_φ	bulk rotation angular frequency, before (5)
$\tilde{v}_\parallel$	$v_\parallel$ in rotating frame, (10)
ψ	flux function, see (1) and (2)

Table 1. Definitions of some commonly used symbols.

2. Single-particle confinement

From a single-particle point of view, the addition of a toroidal field has a lot of apparent advantages for a centrifugal plasma trap, as we derive in this section: The particle orbits, governed by constants of the motion (Sec. 2.1), allow one to retain good centrifugal confinement at smaller applied voltage (Sec. 2.2). If the axial magnetic field is not too small, then newly-ionized ions are confined and are substantially heated during their first bounce orbit (Sec. 2.3). The physics underlying the corresponding parallel acceleration may be inferred from the detailed lab-frame energy balance (Sec. 2.4). The single-particle confinement properties compare favorably to the reference case of a centrifugal trap with purely axial magnetic field (Sec. 2.5). Unfortunately, as we will see in Sec. 3, MHD equilibrium constraints effectively prevent us from gaining these advantages, at least for a beta-limited mirror plasma.

2.1. Single-particle motion

Let's consider particle motion in a system with time-independent, axisymmetric fields $\boldsymbol{B}$ and $\boldsymbol{E} = -\nabla\phi$. Although the problem can be elegantly addressed in a rotating frame [1], we will use the lab frame for physical transparency.

In our simple-cylindrical coordinates (R, φ, z), the magnetic field may be written as

$$\boldsymbol{B} = I\nabla\varphi + \nabla\psi \times \nabla\varphi, \tag{1}$$

for axisymmetric functions $I(R, z)$ and

$$\psi(R, z) \doteq \int_0^R \mathrm{d}R'\, R' B_z. \tag{2}$$

Single-particle motion under the resulting Lorentz force exactly conserves an energy H and canonical angular momentum $\mathcal{P}_\varphi$ given by

$$H = Z_s e\phi + \frac{1}{2} m_s v^2 \approx Z_s e\phi + \frac{1}{2} m_s (v_\parallel^2 + v_E^2) + \mu B, \tag{3}$$

$$\mathcal{P}_\varphi = Z_s e\psi + m_s R v_\varphi \approx Z_s e\psi + m_s R (b_\varphi v_\parallel + v_{E\varphi}), \tag{4}$$

with $b_\varphi \doteq \hat{\boldsymbol{b}} \cdot \hat{\boldsymbol{\varphi}} = I/BR$ and $v_{E\varphi} \doteq \boldsymbol{v}_E \cdot \hat{\boldsymbol{\varphi}}$. The exact forms are given in terms of total particle velocity $\boldsymbol{v}$, with $v_\varphi = \hat{\boldsymbol{\varphi}} \cdot \boldsymbol{v}$. For the approximate forms, and through the rest of Sec. 2, we assume the Larmor radius is small relative to system length scales. (To relax that approximation, one may use higher-order approximate forms for the invariants [12], or simply integrate the particle motion numerically [13].) Since we allow strong electric field $v_E \gtrsim v_{\mathrm{ti}}$, the adiabatically conserved magnetic moment μ must be defined such that μB is the perpendicular kinetic energy in the $\boldsymbol{E} \times \boldsymbol{B}$-drifting frame [14].

Although we allow a supersonic azimuthal rotation, meaning v_φ up to an order-unity multiple of v_{ti}, we will still assume that the corresponding gyroradius is small, even evaluated with only the axial field, $\rho_{\varphi,z}/\ell \ll 1$ for $\rho_{\varphi,z} \doteq m_s v_\varphi / Z_s e B_z$ and characteristic system length ℓ. This implies that any given particle's radial position never strays far from $\psi \approx \psi_0 \doteq \mathcal{P}_\varphi / Z_s e$: set $(\Delta R)_\mathrm{o} \partial_R \psi \approx \psi_1 \doteq \psi - \psi_0 = -m_s R v_\varphi / Z_s e$ to see that $(\Delta R)_\mathrm{o} \approx -\rho_{\varphi,z}$. We can therefore approximately evaluate most functions at $\psi = \psi_0$. However, we must retain the corrections to $Z_s e\phi$ in H: we will see that $v_\varphi \sim (\partial_R \phi)/B_z$, which means that $Z_s e\phi(\psi) - Z_s e\phi(\psi_0) \sim Z_s e \rho_{\varphi,z} \partial_R \phi \sim m_s v_\varphi^2$ is comparable with the leading-order kinetic energy.

The small-gyroradius approximation also implies that the potential is approximately a flux function: Due to electrons' small mass, the centrifugal force is negligible for them, so their parallel flux is governed by a balance between their parallel pressure gradient and the parallel electric force. This constrains the parallel potential variation $\phi_\sim$ to take a value of order the electron temperature $\phi_\sim \sim T_\mathrm{e}/e$ [15]. This is much smaller than typical values of the total potential ϕ, with $\phi_\sim/\phi \sim T_\mathrm{e}/e\ell\partial_R\phi \sim (Z_\mathrm{i} T_\mathrm{e}/T_\mathrm{i})(v_{\mathrm{ti}}^2/v_\varphi^2)(\rho_{\varphi,z}/\ell)$. For simplicity, we will neglect $\phi_\sim$ altogether in the main text, and, through the rest of Sec. 2, we will focus solely on the confinement of ionic species. For a derivation including $\phi_\sim$ and parallel electron confinement, see Appendix A.

2.2. Single-particle orbits

In this section, we will evaluate the classes of ion orbits that are confined, for the geometry and orderings laid out in Sec. 2.1.

Recalling our simplifying assumption that the potential is a flux function $\phi = \phi(\psi)$, we may define a flux-function angular frequency $\omega_\varphi \doteq \partial_\psi \phi$. Also using (1), we can evaluate

$$B^2 = (I^2 + |\nabla\psi|^2)/R^2, \tag{5}$$

$$v_{E\varphi} = \boldsymbol{v}_E \cdot \hat{\boldsymbol{\varphi}} = (1 - b_\varphi^2)\omega_\varphi R, \tag{6}$$

$$v_E^2 = \boldsymbol{v}_E \cdot \boldsymbol{v}_E = (1 - b_\varphi^2)\omega_\varphi^2 R^2. \tag{7}$$

One may then straightforwardly obtain the approximate axial (R, z) orbits, using the invariants μ, H, $\mathcal{P}_\varphi$ and the small-gyroradius ordering. First, expand $\psi = \psi_0 + \psi_1$ with $\psi_0 = \mathcal{P}_\varphi / Z_s e$ and $\psi_1 \approx -m_s R(b_\varphi v_\parallel + v_{E\varphi})/Z_s e$. In H, we may then evaluate all spatial functions at ψ_0, except the potential, which

requires the first-order correction $Z_s e\phi(\psi) \approx Z_s e\phi_0 + Z_s e\omega_\varphi \psi_1$, with $\phi_0 \doteq \phi(\psi_0)$. We can then expand the Hamiltonian, with all spatial functions evaluated at $\psi = \psi_0$:

$$H - Z_s e\phi_0 \approx \frac{1}{2} m_s \left(v_\parallel - b_\varphi \omega_\varphi R\right)^2 - \frac{1}{2} m_s \omega_\varphi^2 R^2 + \mu B. \quad (8)$$

The last two terms here provide the centrifugal and mirror confinement. To interpret the first term on the right-hand side (RHS), consult Fig. 1 and note that

$$b_\varphi \omega_\varphi R \hat{\boldsymbol{b}} + \boldsymbol{v}_E = \omega_\varphi R \hat{\boldsymbol{\varphi}} \quad (9)$$

to see that

$$\tilde{v}_\parallel \doteq v_\parallel - b_\varphi \omega_\varphi R \quad (10)$$

is the parallel velocity in the frame rigidly rotating azimuthally with angular frequency $\omega_\varphi = -E_R/B_z R$. The axial (in the R, z plane) velocity of a particle is straightforwardly found from $v_\parallel \hat{\boldsymbol{b}} + \boldsymbol{v}_E - \omega_\varphi R \hat{\boldsymbol{\varphi}} = \tilde{v}_\parallel \hat{\boldsymbol{b}}$, so the turning points occur when $\tilde{v}_\parallel = 0$. If we evaluate $(H - Z_s e\phi_0)$ in terms of its value at an initial axial position $z = z_I$, which we will label with a subscript I, then a particle's $\tilde{v}_\parallel$ is given as a function of z (at fixed ψ_0) as

$$\frac{1}{2} m_s \tilde{v}_\parallel^2 \approx \frac{1}{2} m_s \tilde{v}_{\parallel I}^2 - \frac{1}{2} m_s \omega_\varphi^2 (R_I^2 - R^2) - \mu(B - B_I). \quad (11)$$

A particle is therefore confined as long as $\tilde{v}_{\parallel I}^2 < \omega_\varphi^2 (R_I^2 - R_{\min}^2) + 2\mu(B_{\max} - B_I)/m_s$.

To see the effect of nonzero $B_\varphi = \boldsymbol{B} \cdot \hat{\boldsymbol{\varphi}}$ on the required voltage, let's focus on the centrifugal potential term, which is generally the larger term for supersonic rotation $\omega_\varphi R > v_{\text{ti}}$. The radial potential gradient is $\partial_R \phi = \omega_\varphi \partial_R \psi = \omega_\varphi R B_z$. One can therefore reduce the applied voltage at fixed centrifugal confinement, as long B_z is reduced by the same factor as $(\partial_R \phi)$. This can be done at fixed total magnetic field strength, if one increases B_φ^2 to cancel the reduction in B_z^2. Physically, this follows because the trapped particles must rotate azimuthally with the precession speed, which is larger than v_E when $B_\varphi \neq 0$, as is sketched in Fig. 1. This possible reduction in applied voltage is the principal motivation to add a strong azimuthal field to a centrifugal mirror machine. Unfortunately, though, we will see in Sec. 3 that the radial plasma pressure confinement is only due to the magnetic pressure from B_z^2, rather than the total field strength B^2. So, for a mirror at MHD-equilibrium beta limits, one would be unable to reduce B_z at all, no matter how much B_φ was added. In this case, the applied voltage could also not be reduced at all, and would need to stay at its original value. (See a specific numerical example in Appendix A.1)

2.3. Newly-ionized particles

In Sec. 2.2, we saw that the trap geometry from Sec. 2.1 confines particles that are rotating azimuthally with an angular velocity around ω_φ. Much of that angular velocity may come from parallel motion, in principle allowing one to reduce the applied voltage. But will newly ionized ions be accelerated to the necessary range of azimuthal velocities? In this section, we will find that classical and neoclassical polarization do indeed confine and accelerate newly ionized particles, when the geometry satisfies certain conditions. The derivation also clarifies several distinct length and time scales that are important for the confinement.

In the $\boldsymbol{E} \times \boldsymbol{B}$-drifting frame, the electric force $-Z_s e \nabla\phi = -Z_s e \omega_\varphi \nabla\psi$ is canceled by the magnetic force of the frame drift $Z_s e \boldsymbol{v}_E \times \boldsymbol{B} = Z_s e \omega_\varphi \nabla\psi$. In our small-gyroradius limit, the particle trajectory then evolves under the simple magnetic force for nearly-constant magnetic field. In the drifting frame, it undergoes a simple circular gyro-orbit with gyrofrequency $\Omega_s = Z_s e B/m_s$ and gyroradius $v_\perp m_s/Z_s e B$ for $v_\perp \doteq (2\mu B/m_s)^{1/2}$, the shortest confinement-related time and length scales. At first glance, a newly ionized particle looks different—initially approximately stationary, it is accelerated in the direction of the electric force until the magnetic force bends its trajectory enough to overpower the electric force and return it to its starting radius, where it is momentarily stationary. However, this cycloid path is in fact just a special case of the simple gyro-orbit, with $v_\perp = v_E$ and with gyrocenter shifted $v_E m_s/Z_s e B$ down $\nabla\phi$ from the ionization location. Within the first gyro-period, the new particle is therefore drifting with gyro-center velocity $\boldsymbol{v}_E$ and magnetic moment satisfying $\mu B \approx \frac{1}{2} m_s v_E^2$ [9]. However, this acceleration is purely perpendicular, and leaves the lab-frame parallel velocity $v_\parallel$ near zero.

Is this new ion also confined in the parallel direction? This orbit is a special case of the orbits from Sec. 2.2, with initial values $\mu B \approx \frac{1}{2} m_s v_E^2$ and with $\tilde{v}_\parallel \approx 0 - b_\varphi \omega_\varphi R$. Recalling (11), and assuming the minimum of R and maximum of B occur in the same place, the new ion will be confined if $\frac{1}{2} m_s \tilde{v}_{\parallel I}^2 < \frac{1}{2} m_s \omega_\varphi^2 (R_I^2 - R_{\min}^2) + \mu(B_{\max} - B_I)$. Recalling (7) and canceling a common factor of $\frac{1}{2} m_s \omega_\varphi^2 R_I^2$, this criterion will be met when

$$(1 - b_\varphi^2)_I > \frac{R_{\min}^2}{R_I^2} \frac{B_I}{B_{\max}}. \quad (12)$$

Noting that $(1 - b_\varphi^2)_I \geq B_{z,I}^2/B_I^2$ and that we expect at least $B_I/B_{\max} \lesssim R_{\min}/R_I$,[2] equation (12) will be

[2] MHD equilibrium requires that I is a function of ψ alone, see (34). Assume $B_R^2 \ll B_z^2$ and $B_z(R, z) \approx B_z(z)$. Eq. (2) reduces to $\psi(R, z) \approx B_z(z) R^2/2$. Then, defining a function $R(z)$ such that $\psi(R(z), z) = \psi_0$, we may evaluate $B_z(z) = 2\psi_0/R^2(z)$

satisfied if $B_{z,I}^2/B_I^2 > (R_{\min}^3/R_I^3)$. New particles will therefore generally be confined as long as (B_z/B) in the bulk of the trap is no smaller than $(R_{\min}/R_I)^{3/2}$, which represents a non-trivial but manageable constraint on our choice of trap magnetic geometry.

The rotating-frame parallel kinetic energy of new, confined ions is then around $\frac{1}{2}m_s\tilde{v}_\parallel^2 \sim \frac{1}{2}m_s b_\varphi^2\omega_\varphi^2 R^2$. If the azimuthal field is stronger than the axial field, then this initial parallel in-frame kinetic energy is larger than the perpendicular in-frame kinetic energy $\mu B \sim \frac{1}{2}m_s v_E^2 \sim \frac{1}{2}m_s(1-b_\varphi^2)\omega_\varphi^2 R^2$. Also assuming supersonic rotation, we have $\tilde{v}_\parallel^2 \sim \omega_\varphi^2 R^2 \sim M_{\rm i}^2 v_{\rm ti}^2$ for $M_{\rm i}$ greater than unity, so we expect collisions to generally scatter these new ions to smaller $\tilde{v}_\parallel^2$, thus deeper parallel confinement.

The parallel heating of the new ions may be seen as a form of neoclassical polarization: To first order, the particle is located at $\psi = \psi_0 - m_s R(b_\varphi\tilde{v}_\parallel + \omega_\varphi R)/Z_s e$. At any given point in z on a specific particle's bounce orbit, the sign of $\tilde{v}_\parallel$ will take both positive and negative signs, depending on the direction of axial motion of the particle. The introduction of an azimuthal field has thus brought in a finite drift-orbit width $\mp m_s b_\varphi\tilde{v}_\parallel/Z_s e B_z$, of order $\rho_{\varphi,z}$. For mostly-azimuthal magnetic field ($B_z < B$) and $v_\perp \sim \tilde{v}_\parallel$, this is larger than the true gyroradius, analogously to banana orbits in tokamaks. The frequency scale for this confinement is $\sim b_z\tilde{v}_\parallel/\ell$, the inverse of the bounce time, with characteristic system length ℓ. This is slower than the gyrofrequency by a factor of the gyroradius over the scale length. In the presence of collisions, this finite orbit width will enable neoclassical transport (cf. Appendix A.5). Returning to the case of our newly ionized particle, the orbit begins with $v_\parallel = 0$, thus $\tilde{v}_\parallel = -b_\varphi\omega_\varphi R$ and radial position $\psi = \psi_0 - m_s(1-b_\varphi^2)\omega_\varphi R^2/Z_s e$. When it returns to its starting point it must have $\tilde{v}_\parallel = +b_\varphi\omega_\varphi R$, thus radial position $\psi = \psi_0 - m_s(1+b_\varphi^2)\omega_\varphi R^2/Z_s e$ and lab-frame parallel velocity $v_\parallel = 2b_\varphi\omega_\varphi R$. The gain in parallel kinetic energy, from 0 to $2m_s b_\varphi^2\omega_\varphi^2 R^2$, came from the lost potential energy $Z_s e(\partial_\psi\phi)(\psi_{\rm return}-\psi_I) = -2m_s b_\varphi^2\omega_\varphi^2 R^2$. In the next section, we will take a closer look at the detailed transfer mechanisms.

2.4. Lab-frame energy balance

The parameter bounds for confined orbits are most succinctly calculated in terms of the invariants, as in Secs. 2.2 and 2.3. In this subsection, we will look at the same problem using the guiding-center equations. This will not extend or change our previous results, but it may help to clarify the underlying physical mechanisms.

and, using (1), $B_\varphi(R(z),z) = I(\psi_0)/R$, so

$$\frac{B_I^2}{B_{\max}^2} \approx \frac{I^2(\psi_0)/R_I^2 + 4\psi_0^2/R_I^4}{I^2(\psi_0)/R_{\min}^2 + 4\psi_0^2/R_{\min}^4} = \frac{R_{\min}^2}{R_I^2}\frac{I^2(\psi_0)+4\psi_0^2/R_I^2}{I^2(\psi_0)+4\psi_0^2/R_{\min}^2} \le \frac{R_{\min}^2}{R_I^2}.$$

We will use single-particle guiding-center equations that allow strong $\boldsymbol{E}\times\boldsymbol{B}$ flows $v_E \sim v_{\rm ti}$ [14]. The approximate guiding-center velocity is

$$\boldsymbol{v}_{\rm gc} = v_\parallel\hat{\boldsymbol{b}} + \boldsymbol{v}_E + \boldsymbol{v}_{\perp 1}, \tag{13}$$

in which

$$\boldsymbol{v}_{\perp 1} \doteq \Omega_s^{-1}\hat{\boldsymbol{b}}\times(v_\parallel d_{t0}\hat{\boldsymbol{b}} + d_{t0}\boldsymbol{v}_E + m_s^{-1}\mu\nabla B) \tag{14}$$

for $d_{t0} \doteq (v_\parallel\hat{\boldsymbol{b}} + \boldsymbol{v}_E)\cdot\nabla$. The first-order drift $\boldsymbol{v}_{\perp 1}$ captures the strong-$\boldsymbol{E}\times\boldsymbol{B}$ versions of the curvature drift $\hat{\boldsymbol{b}}\times(v_\parallel d_{t0}\hat{\boldsymbol{b}})/\Omega_s$, polarization drift $\hat{\boldsymbol{b}}\times(d_{t0}\boldsymbol{v}_E)/\Omega_s$, and grad-$B$ drift $\hat{\boldsymbol{b}}\times(\mu\nabla B)/m_s\Omega_s$. Each term in $\boldsymbol{v}_{\perp 1}$ is smaller than the leading-order velocity $(v_\parallel\hat{\boldsymbol{b}} + \boldsymbol{v}_E)$ by one order in gyroradius over scale length. We need only evaluate evolution of $v_\parallel$ to its leading order:

$$m_s d_t v_\parallel = -Z_s e\nabla_\parallel\phi - \mu\nabla_\parallel B + m_s\boldsymbol{v}_E\cdot d_{t0}\hat{\boldsymbol{b}}, \tag{15}$$

with $\nabla_\parallel \doteq \hat{\boldsymbol{b}}\cdot\nabla$.

Equations (13)–(15) approximately conserve the energy given by (3), with individual terms evolving as

$$d_t\frac{1}{2}m_s v_\parallel^2 = -v_\parallel(Z_s e\nabla_\parallel\phi + \mu\nabla_\parallel B) + m_s\boldsymbol{v}_E\cdot v_\parallel d_{t0}\hat{\boldsymbol{b}}, \tag{16}$$

$$d_t\mu B = (v_\parallel\hat{\boldsymbol{b}} + \boldsymbol{v}_E)\cdot\mu\nabla B, \tag{17}$$

$$d_t\frac{1}{2}m_s v_E^2 = m_s\boldsymbol{v}_E\cdot d_{t0}\boldsymbol{v}_E, \tag{18}$$

$$d_t Z_s e\phi = v_\parallel Z_s e\nabla_\parallel\phi - \boldsymbol{v}_E\cdot[m_s(v_\parallel d_{t0}\hat{\boldsymbol{b}} + d_{t0}\boldsymbol{v}_E) + \mu\nabla B]. \tag{19}$$

These equations are only accurate to the order of $m_s v_{ts}^3/\ell$, so the right-hand sides of (16)–(18) are only evaluated to their leading order.[3] For (19), we had to keep the correction due to $\boldsymbol{v}_{\perp 1}$, for which we rearranged the triple product as

$$\boldsymbol{v}_{\perp 1}\cdot\nabla Z_s e\phi = -\frac{\hat{\boldsymbol{b}}}{\Omega_s}\times\nabla(Z_s e\phi)\cdot(v_\parallel d_{t0}\hat{\boldsymbol{b}} + d_{t0}\boldsymbol{v}_E + \frac{\mu\nabla B}{m_s}). \tag{20}$$

Let's now consider the parallel confinement of an ion, particularly the special case of a newly ionized ion, looking through (15) term by term, and comparing with the example orbit sketched in Fig. 2. First, since we assume $\phi = \phi(\psi)$, we have $\nabla_\parallel\phi = 0$. Next, we have the standard parallel magnetic mirror force $-\mu\nabla_\parallel B$, which always pushes towards regions of weak B, thus confines the ion towards the midplane and away from the endcaps. For a newly ionized ion, which had $v_\parallel = 0$ at the midplane, this force is transferring energy to the ion's parallel motion $m_s v_\parallel^2/2$ over the entirety of the first half bounce orbit (midplane to endcap and back to midplane). This seems counterintuitive, because the energy comes from the perpendicular kinetic energy (μB), which is also growing in the first quarter orbit (midplane to endcap). The resolution is that the particle is concurrently ∇B-drifting down $\nabla Z_s e\phi$, which is transferring energy from $Z_s e\phi$ into μB

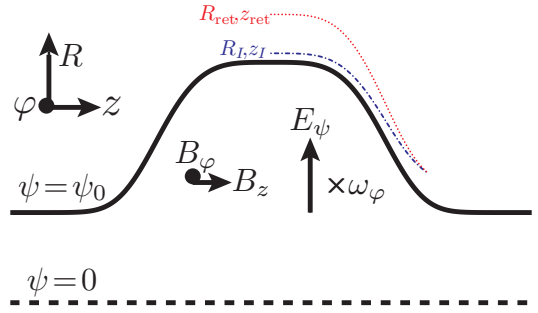

Figure 2. Initial half-bounce orbit of a newly ionized ion, projected onto R, z plane. (In this case, the azimuthal motion is always in the $-\hat{\boldsymbol{\varphi}}$ direction, around the axis of symmetry, $\psi = 0$.) The ion is ionized on the ψ_0 magnetic surface, but due to the initial polarization, the gyro-center starts at (R_I, z_I). The ion's total kinetic energy $\frac{1}{2}m_s(v_\parallel^2 + v_E^2) + \mu B$ comes from the potential energy lost by the radial shift from ψ_0 to its current radial position $(\psi_0 + \psi_1)$, the thin-line orbit that is sketched. At (R_I, z_I), $v_\parallel^2 = 0$ and $\mu B = \frac{1}{2}m_s v_E^2$. Over the first quarter orbit (dash-dotted blue), the ion moves from (R_I, z_I) out to the bounce point near the positive-z endcap, then in the second quarter orbit (dotted red) it returns to the midplane but at greater $R = R_{\rm ret}$. Over this whole time, $\tilde{v}_\parallel$ is becoming increasingly negative, corresponding to an increase in $\frac{1}{2}m_s v_\parallel^2$, with the net increase in total kinetic energy coming from potential energy $Z_s e\phi$ released by the first-order drifts $\boldsymbol{v}_{\perp 1}$ down $\nabla\phi$.

via the $\boldsymbol{v}_E \cdot \mu\nabla B$ term, and $|\boldsymbol{v}_E \cdot \mu\nabla B| > |v_\parallel \hat{\boldsymbol{b}} \cdot \mu\nabla B|$ for the first quarter orbit.

Centrifugal confinement is in fact electrostatic confinement mediated by the last term of (15), but it takes a little algebra to see this: Equations (1) and (5) jointly imply

$$\frac{\hat{\boldsymbol{b}}}{B}\times\nabla\psi = \frac{1}{B^2}[I(I\nabla\varphi - \boldsymbol{B}) + |\nabla\psi|^2\nabla\varphi] = R(\hat{\boldsymbol{\varphi}} - b_\varphi\hat{\boldsymbol{b}}), \quad (21)$$

an identity commonly used in neoclassical theory [16]. In our axisymmetric geometry with $\phi = \phi(\psi)$, we find that[4]

$$\boldsymbol{v}_E = \frac{\hat{\boldsymbol{b}}}{B} \times \nabla\phi = \frac{\hat{\boldsymbol{b}}}{B} \times \omega_\varphi \nabla\psi = \omega_\varphi R(\hat{\boldsymbol{\varphi}} - b_\varphi\hat{\boldsymbol{b}}), \quad (22)$$

$$d_{t0} \doteq (v_\parallel\hat{\boldsymbol{b}} + \boldsymbol{v}_E)\cdot\nabla = (\omega_\varphi R\hat{\boldsymbol{\varphi}} + \tilde{v}_\parallel\hat{\boldsymbol{b}})\cdot\nabla, \quad (23)$$

$$d_{t0}\hat{\boldsymbol{b}} = [(\omega_\varphi R\hat{\boldsymbol{\varphi}} + \tilde{v}_\parallel\hat{\boldsymbol{b}})\cdot\nabla]\hat{\boldsymbol{b}} = \omega_\varphi\hat{\boldsymbol{z}}\times\hat{\boldsymbol{b}} + \tilde{v}_\parallel(\hat{\boldsymbol{b}}\cdot\nabla)\hat{\boldsymbol{b}}, \quad (24)$$

$$\boldsymbol{v}_E\cdot d_{t0}\hat{\boldsymbol{b}} = \omega_\varphi R\hat{\boldsymbol{\varphi}}\cdot d_{t0}\hat{\boldsymbol{b}} = \nabla_\parallel(\omega_\varphi^2 R^2/2) + \tilde{v}_\parallel\omega_\varphi\nabla_\parallel(b_\varphi R). \quad (25)$$

For centrifugally confined particles, we expect $|\tilde{v}_\parallel| < \omega_\varphi R$, so the first term on the RHS of (25) is the larger.[5] This term accelerates a particle's parallel velocity towards large radius, thus acts to confine a particle from the endcaps back towards the central region. In the case of the newly ionized particle, this corresponds to an energy transfer into $\frac{1}{2}m_s v_\parallel^2$. Recalling the derivation of (19), this energy comes from potential energy freed by the generalized curvature drift,

$$\Omega_s^{-1}\hat{\boldsymbol{b}}\times v_\parallel d_{t0}\hat{\boldsymbol{b}} = \Omega_s^{-1} v_\parallel[\omega_\varphi\hat{\boldsymbol{z}} + \tilde{v}_\parallel(\nabla\times\hat{\boldsymbol{b}})]_\perp, \quad (26)$$

where the subscript $\perp$ indicates the perpendicular projection, e.g. $\hat{\boldsymbol{z}}_\perp = \hat{\boldsymbol{z}} - (\hat{\boldsymbol{b}}\cdot\hat{\boldsymbol{z}})\hat{\boldsymbol{b}}$.

2.5. Purely axial field

For comparison purposes, we consider a centrifugal mirror with no azimuthal field. Mathematically, this is just a special case of the analysis we have already done—the equations of the previous sections continue to hold here, simply taking the special case $I = 0$, thus also $b_\varphi = 0$ and $\tilde{v}_\parallel = v_\parallel$. However, this special case serves as a useful point of reference, connecting with current and past experiments including Ixion, a small, pulsed device that generated a cool but supersonically-rotating and axially-confined plasma back in the 1960s [2], and the larger Maryland Centrifugal eXperiment (MCX/CMFX)[3], which demonstrated momentum confinement times longer than an MHD-instability growth time [8] and strong pressure gradients in the parallel direction [5].

The key physical difference is a clear separation of the azimuthal rotation, which consists to leading order only of the $\boldsymbol{E}\times\boldsymbol{B}$ drift $\boldsymbol{v}_E = \omega_\varphi R\hat{\boldsymbol{\varphi}}$, from the parallel flow, $v_\parallel\hat{\boldsymbol{b}} \perp \hat{\boldsymbol{\varphi}}$. When we consider orbit confinement, as in Sec. 2.2, this means that the parallel velocity is the same in the rotating frame and in the lab frame, $\tilde{v}_\parallel = v_\parallel$. The criterion for orbit confinement remains that from (11), but it may here be applied directly to the lab-frame parallel velocity, so a particle is confined when $v_{\parallel I}^2 < \omega_\varphi^2(R_I^2 - R^2) + 2\mu(B - B_I)/m_s$. Unlike in Sec. 2.3, here newly ionized ions are trivially confined, since their simple gyromotion is still immediately accelerated to $\mu B = m_s v_E^2/2$, but their near-zero lab-frame parallel velocity $v_\parallel = 0$ now implies an equally small rotating-frame parallel velocity $\tilde{v}_\parallel = 0$. Put another way, this special case trivially satisfies the magnetic-geometry requirement given by (12).

[3] Consistent with the analysis at the end of Sec. 2.1, we assume that $\nabla_\parallel\phi \sim T_e/\ell e$ is one order smaller than its nominal order.

[4] Use the facts that $|\hat{\boldsymbol{b}}|^2 = 1$, $\hat{\boldsymbol{b}}\cdot d_{t0}\hat{\boldsymbol{b}} = d_{t0}|\hat{\boldsymbol{b}}|^2/2 = 0$, and $R\hat{\boldsymbol{\varphi}}\cdot[(\hat{\boldsymbol{b}}\cdot\nabla)\hat{\boldsymbol{b}}] = (\hat{\boldsymbol{b}}\cdot\nabla)(b_\varphi R)$.

[5] For a newly ionized particle, the two terms may be comparable in size, but the net effect is still definitely confining. To see this, note first that $v_z \approx (v_\parallel\hat{\boldsymbol{b}} + \boldsymbol{v}_E)\cdot\hat{\boldsymbol{z}} = \tilde{v}_\parallel b_z$, then evaluate the leading order $m_s d_t\tilde{v}_\parallel = m_s d_t v_\parallel - m_s\omega_\varphi d_t(b_\varphi R)$, with $d_t v_\parallel$ from (15) and (25), and using axisymmetry and (23) to evaluate the leading order $d_t(b_\varphi R) = \tilde{v}_\parallel\nabla_\parallel(b_\varphi R)$, thus

$$m_s d_t\tilde{v}_\parallel = -Z_s e\nabla_\parallel\phi - \mu\nabla_\parallel B + m_s\nabla_\parallel(\omega_\varphi^2 R^2/2).$$

The first term on the RHS is zero for $\phi = \phi(\psi)$, and the other two definitely push away from the endcaps and towards the midplane.

The detailed physical mechanisms of confinement are also basically unchanged. Consider the equations of Sec. 2.4, which continue to apply here, in the special case $I = 0$ thus $b_\varphi = 0$ and $\tilde{v}_\parallel = v_\parallel$. Parallel confinement is enforced by the terms on the RHS of (15). Since we still assume $\phi = \phi(\psi)$, the first term $\propto \nabla_\parallel \phi$ is zero. The magnetic mirror term $-\mu\nabla_\parallel B$ again acts as a confining force, pushing the particle towards weak B, thus towards the device midplane $z = 0$. However, in this special case the energy balance is simpler: Since $\boldsymbol{v}_E \parallel \hat{\boldsymbol{\varphi}} \perp \nabla B$, equation (17) simplifies to $d_t \mu B = v_\parallel \mu \nabla_\parallel B$, so energy is taken from $\frac{1}{2}m_s v_\parallel^2$ to μB for outgoing particles (increasing B), and from μB to $\frac{1}{2}m_s v_\parallel^2$ for incoming particles. This energy transfer is confining in this case, because the axial motion is now purely parallel, thus the turning points occur when $v_\parallel = 0$.

Centrifugal confinement again follows from the last term of (15), and remains an electrostatic effect, though somewhat simplified: With $b_\varphi = 0$, equation (25) simplifies to $\boldsymbol{v}_E \cdot d_{t0}\hat{\boldsymbol{b}} = \nabla_\parallel(\omega_\varphi^2 R^2/2)$, so the centrifugal confinement force is no longer modified by any $\tilde{v}_\parallel$ dependence. Physically, the strong-$\boldsymbol{E}\times\boldsymbol{B}$ curvature drift from (26) has a corresponding simplification. The second term of the drift may now be written as $\Omega_s^{-1} v_\parallel^2 (\nabla \times \hat{\boldsymbol{b}})$, and it is purely azimuthal. This part of the drift is therefore orthogonal to $Z_s e \nabla\phi$, so it cannot transfer energy between $\frac{1}{2}m_s v_\parallel^2$ and the potential. The first term is now entirely due to the $(\boldsymbol{v}_E \cdot \nabla)\hat{\boldsymbol{b}}$ portion of $d_{t0}\hat{\boldsymbol{b}}$, and it is actually mostly radial, since in our simplified magnetic geometry

$$\Omega_s^{-1} v_\parallel \omega_\varphi \hat{\boldsymbol{z}}_\perp = \Omega_s^{-1} v_\parallel \omega_\varphi (-b_z b_R \hat{\boldsymbol{R}} + b_R^2 \hat{\boldsymbol{z}}) \tag{27}$$

and we expect $b_R \ll b_z \approx 1$ for a typical elongated device. The potential energy gain due to this drift, $\Omega_s^{-1} v_\parallel \omega_\varphi \hat{\boldsymbol{z}}_\perp \cdot Z_s e \nabla\phi = -m_s v_\parallel \hat{\boldsymbol{b}} \cdot \nabla(\omega_\varphi^2 R^2/2)$, indeed comes from $\frac{1}{2}m_s v_\parallel^2$ via the $\boldsymbol{v}_E \cdot d_{t0}\hat{\boldsymbol{b}}$ term, thus slowing an outgoing particle (motion towards small R) and accelerating an incoming particle.

Previous work has pointed out that a centrifugal mirror with purely axial field should not exhibit neoclassical transport [3, 9]. This may appear inconsistent with the clear role of a radial drift-orbit excursion ($\psi_1 \neq 0$) in the centrifugal confinement. However, the magnetic geometry of this section should in fact be free of neoclassical transport, at least in the conventional sense. The basic reason is that the orbit excursion, although finite, is velocity-independent. Collisions alter a particle's velocity at a fixed point in space. However, in this $B_\varphi = 0$ case, a collision-induced velocity shift does not cause a change in the spatial trajectory of the particle, except possibly its (insignificant) azimuthal position.

However, this arrangement is the most demanding one when it comes to the applied-voltage requirements. As in the finite-B_φ case, one here has $\partial_R\phi = \omega_\varphi \partial_R \psi = \omega_\varphi R B_z$. With $B_\varphi = 0$, and assuming a reasonably elongated trap, we have $B \approx B_z$, which means that we are unable to reduce B_z without also reducing the confining magnetic field.

3. MHD equilibrium

In Section 2, we found that the applied voltage needed for centrifugal confinement could be reduced, if you were able to reduce the axial magnetic field. Unfortunately, in this geometry, only the axial magnetic field is able to confine the plasma pressure. In this section, we will derive a modest generalization of the Grad-Shafranov equation (Sec. 3.1), find the resulting constraints on the effect of B_φ (Sec. 3.2), and tie these conclusions to their physical origins in single-particle motion (Sec. 3.3)

3.1. Centrifugal-mirror equilibrium equations

For this derivation, we will use the ideal MHD equations [17], with mass density ρ_m, mass-flow velocity $\boldsymbol{u}$, plasma pressure p, and current density $\boldsymbol{j}$.[6] We assume that the fields and plasma are axisymmetric and time-independent, implying $\boldsymbol{E} = -\nabla\phi$ and $\boldsymbol{B}$ given by (1). Since we use the ideal Ohm's Law $\boldsymbol{E} + \boldsymbol{u}\times\boldsymbol{B} = 0$, we have $\hat{\boldsymbol{b}} \cdot \nabla\phi = 0$.[7] Together with axisymmetry $\partial_\varphi \phi = 0$, this implies that the potential is a flux function $\phi = \phi(\psi)$, thus we may again define the flux-function angular frequency $\omega_\varphi(\psi) = \partial_\psi \phi$. Recalling (22), the perpendicular components of the ideal Ohm's Law then imply

$$\boldsymbol{u} - u_\parallel \hat{\boldsymbol{b}} = \frac{\hat{\boldsymbol{b}}}{B} \times (\boldsymbol{u}\times\boldsymbol{B}) = \boldsymbol{v}_E = \omega_\varphi R(\hat{\boldsymbol{\varphi}} - b_\varphi \hat{\boldsymbol{b}}), \tag{28}$$

for $u_\parallel \doteq \boldsymbol{u}\cdot\hat{\boldsymbol{b}}$. With $\tilde{u}_\parallel \doteq u_\parallel - b_\varphi \omega_\varphi R$, the mass-density flux is

$$\rho_\mathrm{m}\boldsymbol{u} = \rho_\mathrm{m}(\omega_\varphi R \hat{\boldsymbol{\varphi}} + \tilde{u}_\parallel \hat{\boldsymbol{b}}), \tag{29}$$

so mass conservation implies

$$0 = \nabla\cdot(\rho_\mathrm{m}\boldsymbol{u}) = \nabla\cdot(\rho_\mathrm{m}\tilde{u}_\parallel\hat{\boldsymbol{b}}) = \boldsymbol{B}\cdot\nabla(\rho_\mathrm{m}\tilde{u}_\parallel/B). \tag{30}$$

We are only interested in configurations that confine the plasma in the parallel direction, which means that $\rho_\mathrm{m}\tilde{u}_\parallel$ must go to zero in the endcaps, thus by (30) we must have $\tilde{u}_\parallel = 0$ everywhere, so $\boldsymbol{u} = \omega_\varphi R \hat{\boldsymbol{\varphi}}$.

We are now ready to consider force balance,[8]

$$\rho_\mathrm{m}(\boldsymbol{u}\cdot\nabla)\boldsymbol{u} = \boldsymbol{j}\times\boldsymbol{B} - \nabla p. \tag{31}$$

[6] The generalized Hall-MHD formulation has interesting implications for centrifugal mirrors [18], but does not significantly alter the results of this section.

[7] See a treatment including the parallel electric field in Appendix A.

[8] Here we assume an isotropic plasma pressure, which should approximately hold for a magnetized, supersonically rotating mirror: Recall from Sec. 2.1 that ions stay close to a reference magnetic surface $\psi = \psi_0$. From (11), and here using subscript I

First evaluate Ampère's Law for $\boldsymbol{B}$ from (1), yielding

$$\mu_0 \boldsymbol{j} = \nabla \times \boldsymbol{B} = \nabla I \times \nabla\varphi - (\Delta^* \psi)\nabla\varphi \tag{32}$$

for $\Delta^*\psi \doteq \partial_R^2\psi - R^{-1}\partial_R\psi + \partial_z^2\psi$ [17]. The inertial term is

$$\rho_\mathrm{m}(\boldsymbol{u}\cdot\nabla)\boldsymbol{u} = \rho_\mathrm{m}\omega_\varphi\partial_\varphi(\omega_\varphi R\hat{\boldsymbol{\varphi}}) = -\rho_\mathrm{m}\omega_\varphi^2\nabla(R^2/2). \tag{33}$$

The azimuthal component ($\mu_0 R\hat{\boldsymbol{\varphi}}\cdot$) of (31) reduces to

$$0 = \mu_0 R\hat{\boldsymbol{\varphi}}\cdot\boldsymbol{j}\times\boldsymbol{B} = \boldsymbol{B}\cdot\nabla I, \tag{34}$$

so I is a flux function $I(\psi)$. The parallel component of force balance,

$$\nabla_\parallel p = \rho_\mathrm{m}\omega_\varphi^2\nabla_\parallel(R^2/2) = \rho_\mathrm{m}\nabla_\parallel(\omega_\varphi^2 R^2/2), \tag{35}$$

determines the pressure up to an arbitrary flux function, physically capturing the parallel centrifugal confinement. The detailed solution depends on the equation of state, which relates p and ρ_m. For example, an (ad hoc) isothermal relation $p = c_\mathrm{s}^2\rho_\mathrm{m}$ for flux-function sound speed $c_\mathrm{s} = c_\mathrm{s}(\psi)$ would lead to $p(\psi,R) = p_I(\psi)\exp\big(\omega_\varphi^2(R^2-R_I^2)/2c_\mathrm{s}^2\big)$. However, we will not make this assumption, since our results do not depend on any specific form for the parallel variation of p. Finally, we will calculate the radial-confinement component $[|\nabla\psi|^{-2}(\nabla\psi)\cdot]$ of (31), which gives us a generalized Grad-Shafranov equation

$$(\Delta^*\psi) = -I'I - \mu_0 R^2[\partial_\psi p - \rho_\mathrm{m}\omega_\varphi^2\partial_\psi(R^2/2)], \tag{36}$$

where $I'(\psi)$ is the derivative of $I(\psi)$ with respect to ψ and where $\partial_\psi \doteq |\nabla\psi|^{-2}(\nabla\psi)\cdot\nabla$.

3.2. Constraints on rotating equilibria

The basic MHD equilibrium force balance directly implies that the azimuthal rotation is limited by the Alfvén speed, as observed in experiment [10]. To see this simply, we can write the $\hat{\boldsymbol{R}}$ component of (31) in the form[9]

$$\partial_R B_z^2 + R^{-2}\partial_R I^2 - 2B_z\partial_z B_R = 2\mu_0(\rho_\mathrm{m}\omega_\varphi^2 R - \partial_R p). \tag{37}$$

For supersonic flows, we expect $\rho_\mathrm{m}\omega_\varphi^2 R > |\partial_R p|$, and for an elongated trap we expect $|\partial_z B_R| < |\partial_R B_z|$. Neglecting the $\partial_R p$ and $\partial_z B_R$ terms altogether, for simplicity, we consider first the case of a centrifugal mirror with only axial field, so $I^2 = 0$. We can integrate the remaining two terms radially from R to some outer-bound radius R_out, rearranging a bit to

$$\frac{B_z^2(R)}{B_z^2(R_\mathrm{out})} \approx 1 - 2\int_R^{R_\mathrm{out}} \frac{\mathrm{d}R'}{R'}\,\frac{(\omega_\varphi R')^2}{B_z^2(R_\mathrm{out})/\mu_0\rho_\mathrm{m}}. \tag{38}$$

Obviously, this must be positive for any physical equilibrium, setting an upper bound on the size of the last term. That term represents a weighted radial average of the ratio of the squared toroidal velocity $(\omega_\varphi R)^2$ to the square of the Alfven speed evaluated with the axial field $B_z^2(R_\mathrm{out})/\mu_0\rho_\mathrm{m}$. Equation (38) thus limits the Alfvénic Mach number, similarly to experiment.

In a case with $B_\varphi = I/R$ larger than B_z, we might expect the second term of (37) to dominate over $\partial_R B_z^2$. If that were true, and still neglecting $\partial_R p$ and $\partial_z B_R$ terms, we could radially integrate the two remaining terms to get

$$\frac{I^2(R)}{I^2(R_\mathrm{out})} \approx 1 - 2\int_R^{R_\mathrm{out}} \frac{\mathrm{d}R'R'}{R_\mathrm{out}^2}\,\frac{(\omega_\varphi R')^2}{B_\varphi^2(R_\mathrm{out})/\mu_0\rho_\mathrm{m}}. \tag{39}$$

Since $I^2 = B_\varphi^2 R^2$ needs to be positive for a physical equilibrium, the RHS again represents a limit on a radial average of the Alfvénic Mach number. However, in (39) the Alfvén speed is evaluated with B_φ, suggesting that one may indeed increase the rotation speed via the addition of an azimuthal field.

Unfortunately, even with the addition of a strong azimuthal field, the axial-field Mach number constraint of (38) continues to apply, as we will now show. The key constraint comes from (32) and (34), which jointly imply that

$$\mu_0\boldsymbol{j} + (\Delta^*\psi)\nabla\varphi = I'\nabla\psi\times\nabla\varphi = I'(\boldsymbol{B} - B_\varphi\hat{\boldsymbol{\varphi}}). \tag{40}$$

In words, the axial (R,z-plane) equilibrium current is just I'/μ_0 times the axial magnetic field. However, any successful trap must confine both ions and electrons in the axial direction, meaning that the axial current density must go to zero in the endcaps. Unfortunately, since I' is a flux function, and since the axial magnetic field must stay nonzero in the endcaps, equation (40) implies that the only way to eliminate the axial current density in the endcaps is to set $I' = 0$. Physically, this is equivalent to stating that the axial current density must be zero, which restricts the azimuthal field to take only its vacuum-field value. This means that the azimuthal field is actually completely unable to contribute to the confining pressure balance, since the $\partial_R I^2$ term in (37) must be zero, equivalently the $I'I$ term in (36) must be zero. The rotation-velocity limit is then set purely by the axial field, as in (38), preventing one from reducing B_z below a rotation-dependent floor, regardless of the value of B_φ.

to indicate the value at the outermost R for the $\psi = \psi_0$ surface, we conclude that ions' motion (at roughly constant ψ) is limited by $\omega_\varphi^2(R_I^2 - R^2) \lesssim \tilde{v}_{\parallel I}^2$, thus $(R_I - R)/R_I \lesssim \tilde{v}_{\parallel I}^2/\omega_\varphi^2 R_I(R_I + R) \sim M_\mathrm{i}^{-2} \ll 1$. Consistent with footnote 2, we expect $(B - B_I)/B_I \sim (R_I - R)/R_I$ to also be small, implying that μ conservation does not lead to a significant pressure anisotropy. For electrons, a similar conclusion follows from confinement by the ambipolar electric field discussed at the end of Sec. 2.1.

[9] This form can also be obtained by multiplying (36) by $2R^{-2}\partial_R\psi = 2B_z/R$, then using (35) and the relation $\partial_R = (\partial_R\psi)\partial_\psi + b_R\nabla_\parallel$.

3.3. Single-particle interpretation of MHD constraints

While the results of Sec. 3.2 are mathematically straightforward, they may appear inconsistent with the single particle results of Sec. 2. In this section, we will resolve the apparent discrepancy with a simple single-particle interpretation of our MHD results.

To begin, we consider the drift motion of electrons and ions in a strongly magnetized, supersonically rotating two-species plasma. Recall (13) and focus first on perpendicular motion. The strongest drift is the $\boldsymbol{E}\times\boldsymbol{B}$ drift, but that is equal for electrons and ions, thus it causes no current. Recalling (22) and (23), the first-order drifts from (14) can be rearranged as

$$\boldsymbol{v}_{\perp 1} = \Omega_s^{-1}\hat{\boldsymbol{b}}\times[(\omega_\varphi R\hat{\boldsymbol{\varphi}}+\tilde{v}_\parallel\hat{\boldsymbol{b}})\cdot\nabla(\omega_\varphi R\hat{\boldsymbol{\varphi}}+\tilde{v}_\parallel\hat{\boldsymbol{b}})+m_s^{-1}\mu\nabla B]. \quad (41)$$

For the supersonically rotating ions, the largest first-order drift is

$$\boldsymbol{v}_{\perp 1} \approx \Omega_\mathrm{i}^{-1}\hat{\boldsymbol{b}}\times[\omega_\varphi R\hat{\boldsymbol{\varphi}}\cdot\nabla(\omega_\varphi R\hat{\boldsymbol{\varphi}})] = -\Omega_\mathrm{i}^{-1}\hat{\boldsymbol{b}}\times\omega_\varphi^2 R\hat{\boldsymbol{R}}. \quad (42)$$

Assuming $T_\mathrm{e}\lesssim T_\mathrm{i}$, the electrons' small mass implies that all of their first-order drift terms are smaller than (42). If the drift from (42) were the ions' only response to the centrifugal force, then we would indeed have $I'\neq 0$, so a plasma with mostly azimuthal $\boldsymbol{B}$ could rotate at the Alfvén speed corresponding to B_φ, as in (39).

However, particle confinement along the field implies a constraint that changes this conclusion: In order for a particle to be confined in the $\hat{\boldsymbol{z}}$ direction, its time-averaged $v_z \doteq \boldsymbol{v}\cdot\hat{\boldsymbol{z}}$ must be zero. Consider an ion with perpendicular drift $\boldsymbol{v}_E+\boldsymbol{v}_{\perp 1}$ with $\boldsymbol{v}_{\perp 1}$ from (42).[10] Recalling (22) and (23), we find

$$(v_\parallel\hat{\boldsymbol{b}}+\boldsymbol{v}_E+\boldsymbol{v}_{\perp 1})\cdot\hat{\boldsymbol{z}} = b_z\tilde{v}_\parallel + b_\varphi\omega_\varphi^2 R/\Omega_\mathrm{i}, \quad (43)$$

so in the time average we expect $\tilde{v}_\parallel \approx -b_\varphi\omega_\varphi^2 R/\Omega_\mathrm{i}b_z$, thus an azimuthal velocity around

$$(v_\parallel\hat{\boldsymbol{b}}+\boldsymbol{v}_E+\boldsymbol{v}_{\perp 1})\cdot\hat{\boldsymbol{\varphi}} = \omega_\varphi R - (b_\varphi^2+b_z^2)\omega_\varphi^2 R/b_z\Omega_\mathrm{i}. \quad (44)$$

We can then calculate the current. The average $\hat{\boldsymbol{z}}$-directed velocity is separately zero for both ions and electrons, so $j_z=0$. For the azimuthal current, both electrons and ions rotate with the net $\boldsymbol{E}\times\boldsymbol{B}$ rotation $\omega_\varphi R\hat{\boldsymbol{\varphi}}$, causing no net current. However, the ions' net centrifugal drift is much larger, so we can estimate the azimuthal current density to be around the ion charge density ($Z_\mathrm{i}e\rho_\mathrm{m}/m_\mathrm{i}$) multiplied by their time-averaged azimuthal velocity minus $\omega_\varphi R$, leading to

$$\boldsymbol{j} \approx -\hat{\boldsymbol{\varphi}}(b_\varphi^2+b_z^2)\rho_\mathrm{m}\omega_\varphi^2 R/b_z B. \quad (45)$$

[10] This first-order drift did not contribute to the MHD mass flux $\rho_\mathrm{m}\boldsymbol{u}$ in (29), even though $\rho_\mathrm{m}\boldsymbol{u}$ is very nearly equal to the ion particle flux, times m_i. The basic reason is that the MHD equations only evaluate the mass flux with leading order $\boldsymbol{u}$. However, as necessitated by a leading-order cancellation, they actually evolve the current density $\boldsymbol{j}$ up to the first-order drifts. See Ref. [14] for a tutorial discussion.

Substituting (45) for $\boldsymbol{j}$ in (32), the axial component gives us $\nabla I = 0$. The azimuthal component then reproduces (36) with $I'=0$, in the supersonic limit, thus neglecting ∇p and taking $B_R^2 \ll B_z^2$.[11] With that, we have reproduced the basic result of Sec. 3.2, from an intuitive single-particle point of view.

4. Conclusions

Although centrifugal mirrors offer many potentially appealing features, they generally require an extremely large applied voltage $Z_\mathrm{i}e\phi/T_\mathrm{i}\sim M_\mathrm{i}(R_0/\rho_\mathrm{i})$, presenting a significant technical challenge for a reactor-scale device (Sec. 1). If one were to modify the centrifugal-mirror geometry by adding a strong azimuthal field B_φ, this could transfer some of the toroidal rotation to a parallel flow (Fig. 1). Indeed, an invariant-based orbit calculation indicates that one could maintain a given confining azimuthal velocity $\omega_\varphi R$ with a smaller applied voltage ϕ if the axial magnetic field B_z were proportionately decreased, even if one maintained the total magnetic field strength by adding B_φ (Sec. 2.2). Further, if some modest geometric restrictions (12) are met, then newly-ionized ions would be confined and experience both significant perpendicular and parallel heating within their first bounce orbit (Sec. 2.3). Physically, the centrifugal confinement and the first-orbit heating are electrostatic effects due to drifts up and down $\nabla\phi$ (Sec. 2.4).

Unfortunately, the MHD equilibrium limits the possible benefits of this configuration. In essence, the fact that the plasma current can not flow in or out through the endcaps of the device restricts the current, like the single-particle drifts (Sec. 3.3), to be oriented in the azimuthal direction, (40) and following. This means that only the axial field can contribute effectively to radial confinement against the centrifugal force, equivalently that the azimuthal velocity is limited roughly to the Alfvén speed evaluated with the axial magnetic field alone (Sec. 3.2). This presents a hard limit on any reduction of B_z, thus of the applied voltage required for a given azimuthal rotation speed.

Acknowledgments

Helpful discussions with N. J. Fisch, A. B. Hassam, Yi-Min Huang, E. J. Kolmes, and C. A. Romero-Talamás, and funding by the US Dept. of Energy, Office of Science, Contract DE-AC02-09CH11466 are gratefully acknowledged.

[11] Equation (11) limits $\omega_\varphi^2(R_I^2-R^2)\lesssim\tilde{v}_{\parallel I}^2$, thus $(R_I-R)/R\lesssim\tilde{v}_{\parallel I}^2/\omega_\varphi^2 R(R_I+R)\sim M_\mathrm{i}^2\ll 1$. For this small radial excursion to be consistent with a system-scale axial ($\hat{\boldsymbol{z}}$-directed) orbit length, we must require $B_R^2\ll B_z^2$.

Appendix A. Electron confinement and axial potential variation

In this appendix, we relax the approximation that the potential is a flux function, exploiting a separation of timescales to evaluate the weak parallel variation of the potential that confines electrons to ensure ambipolar losses.

In Appendix A.1, we discuss the separation of timescales that allow for an approximate solve, using parameters for a proposed centrifugal-mirror fusion device as concrete examples. We then solve approximately in order of decreasing/slowing rates, from cyclotron frequency (Ω_s, Appendix A.2), down through collisionless parallel transit (v_{ts}/ℓ_z, Appendix A.3), collision frequency (ν_s, Appendix A.4), and inverse of confinement time (τ_c^{-1}, Appendix A.5). The dynamics at each frequency scale is constrained by the steady state of all of the faster rate scales.

For definiteness, we assume a geometry like Fig. 2 of Ellis, Hassam, Messer and Osborn (EHMO) [3], namely with a long central confinement region, bounded at some positive and negative z by points z_+ and z_- at which B takes its maximum value B_{ec} and flux-surface radius R takes its minimum value R_{ec}. Beyond these points, there are relatively short endcap regions where R increases and B decreases, but there is no plasma confinement. In this geometry, there is no direct contact of confined-particle orbits with the material insulators at the axial ends of the vessel. Except when otherwise stated, our analysis will focus on the confined-plasma region, that is, on the range of z that contains confined particle orbits.

Appendix A.1. Timescale separation: example parameters

The high degree of confinement required for a centrifugal-mirror fusion reactor leads naturally to designs that feature a separation of timescales. When EHMO proposed the Maryland Centrifugal Torus, they also gave parameters for a possible centrifugal-mirror fusion reactor design point. In this appendix, we use these parameters, listed in Table A1, to give a concrete numerical example of the failure of B_φ to allow a voltage reduction, and to exemplify the frequency orderings that underlie the analysis in the subsequent sections of Appendix A.

Consider first the velocities and voltages implied by the parameters given in Table A1, for comparison with Sec. 1. With $v_{ti} \approx 7.1 \cdot 10^5$m/s, the bulk rotation is around $u_\varphi \approx 4.2 \cdot 10^6$m/s, quite close to the Alfvén speed $v_A \approx 4.6 \cdot 10^6$m/s. Since the proposed configuration would have little or no B_φ, the necessary radial electric field would be $(\partial_R \phi) \approx u_\varphi B \approx 10^7$V/m. Even if this electric field is localized to the plasma region of width (ΔR), this would require a potential difference of over 10^7V, a daunting engineering challenge. The potential difference is much larger than $(T_i/e) = 1.3 \cdot 10^4$V, both because M_i is somewhat larger than unity and because the radial device scale [at least (ΔR)] is much larger than the thermal ion gyroradius $\rho_i \approx 7.1 \cdot 10^{-3}$m, also than the ion skin depth $\lambda_i \approx 4.6 \cdot 10^{-2}$m.

Parameter	Value
n_e	$6 \cdot 10^{19}\mathrm{m}^{-3}$
T_i, T_e	13keV
M_i	6
B	2.6T
R_0	4.4m
(ΔR)	1.1m
ℓ_z	22m

Table A1. Parameters for a centrifugal-mirror fusion-plant design point proposed by EHMO [3], with R_0 and (ΔR) the central radius and radial width of the plasma at the midplane ($z = 0$), and ℓ_z the axial length of the plasma. We take $Z_i = 1$ and m_i to be 2.5 times proton mass, to model a deuterium-tritium mix.

Imagine that we changed the design to add an azimuthal field $B_\varphi = 2.6$T and reduced the axial field to $B_z = 0.26$T, so $B \approx 2.6$T stayed roughly constant, leaving all other parameters the same. If we could do this, the necessary electric field would drop to $(\partial_R \phi) \approx u_\varphi B_z \approx 10^6$V/m, thus the voltage to $\sim 10^6$V, still large but significantly more feasible. The ion thermal gyroradius would stay just as small at $\rho_i \approx 7.1 \cdot 10^{-3}$m, but the system would now have finite banana widths $v_{ti} m_i / Z_i e B_z \approx 7.1 \cdot 10^{-2}$m, small relative to system lengths (but allowing some neoclassical transport). However, no MHD equilibrium could exist, because our beta limit from (38) is substantially exceeded, that is,

$$2 \int_R^{R_{out}} \frac{\mathrm{d}R'}{R'} \frac{(\omega_\varphi R')^2}{B_z^2(R_{out})/\mu_0 \rho_m} \sim 2 \frac{(\Delta R)}{R_0} \frac{u_\varphi^2}{B_z^2/\mu_0 \rho_m} \approx 42 \quad \text{(A.1)}$$

is much larger than unity. Indeed, the original design (without B_φ) is already close to the limit, with $2[(\Delta R)/R_0][u_\varphi^2/(B^2/\mu_0\rho_m)] = 2[(\Delta R)/R_0](u_\varphi^2/v_A^2) \approx 0.42$, leaving almost no room to reduce B_z (and thereby the required voltage difference). This design is an example of a beta-limited configuration.

Let's move on to the timescales, again giving examples using the parameters from Table A1, and thinking back to Sec. 2.3. Perpendicular force balance (Appendix A.2) is established on a gyrofrequency rate $\sim \Omega_s$, with $\Omega_i \approx 1.0 \cdot 10^8 \mathrm{s}^{-1}$ and $\Omega_e \approx 4.6 \cdot 10^{11}\mathrm{s}^{-1}$. Any variation about a collisionless drift orbit varies at the slower parallel transit scale $\sim v_{ts}/\ell_z$, with $(v_{ti}/\ell_z) \approx 3.2 \cdot 10^4 \mathrm{s}^{-1}$ and $(v_{te}/\ell_z) \approx 2.2 \cdot 10^6 \mathrm{s}^{-1}$. The velocity-space dependence of the distribution functions f_s relaxes towards a Maxwellian at the collision rates

ν_s, with $\nu_\mathrm{i} \approx 2.6{\cdot}10^1\mathrm{s}^{-1}$ and $\nu_\mathrm{e} \sim 2.1{\cdot}10^3\mathrm{s}^{-1}$. EHMO's (perhaps optimistic) confinement estimate was $\tau_\mathrm{c}^{-1} \sim \nu_\mathrm{e}(4/M_\mathrm{i}^2)\exp(-M_\mathrm{i}^2/4) \approx 2.9\cdot10^{-3}\mathrm{s}^{-1}$. With these orderings in mind, we will proceed to approximately calculate the behavior at each frequency scale, with each scale restricted by the steady-state constraints from faster scales.

Appendix A.2. Perpendicular force balance (Ω_s)

In this appendix, we will show that axisymmetry and steady-state perpendicular force balance jointly imply that the leading-order potential is a flux function $\phi \approx \phi(\psi)$. For intuition, you may compare with the first gyro-orbit of the newly-ionized ion in Sec. 2.3.

At this frequency scale, we may use the cold fluid momentum equations, also neglecting source terms[12]

$$m_s n_s \partial_t \boldsymbol{u}_s = Z_s e n_s (\boldsymbol{E} + \boldsymbol{u}_s \times \boldsymbol{B}). \tag{A.2}$$

Here n_s and $\boldsymbol{u}_s$ are the the species particle density and fluid flow velocity, related to the MHD variables via $\rho_\mathrm{m} = \sum_s n_s m_s$ and $\boldsymbol{u} = \sum_s n_s m_s \boldsymbol{u}_s$. At this level, just as for single-particle dynamics, we see that the (species-independent) steady-state balance is

$$\boldsymbol{u}_{s\perp} = (\hat{\boldsymbol{b}}/B) \times (\boldsymbol{u}_s \times \boldsymbol{B}) = (\boldsymbol{E} \times \boldsymbol{B})/B^2 = \boldsymbol{v}_E, \tag{A.3}$$

and any imbalance ($\boldsymbol{u}_{s\perp} - \boldsymbol{v}_E \neq 0$) triggers rapid evolution $\partial_t \boldsymbol{u}_{s\perp} \sim Z_s e(\boldsymbol{u}_s \times \boldsymbol{B})/m_s \sim \Omega_s \boldsymbol{u}_{s\perp}$.

With axisymmetry, the azimuthal ($R\hat{\boldsymbol{\varphi}}\cdot$) component of (A.2) is

$$m_s \partial_t (R u_{s\varphi}) = -Z_s e \boldsymbol{u}_s \cdot \nabla\psi, \tag{A.4}$$

so in steady state (here meaning: rates slow compared to Ω_s), we expect the velocity to lay within the flux surface ($\boldsymbol{u}_s \cdot \nabla\psi = 0$). Also recalling (A.3), we see that $\boldsymbol{u}_s \cdot \nabla\psi = \boldsymbol{u}_{s\perp} \cdot \nabla\psi = \boldsymbol{v}_E \cdot \nabla\psi$, so with axisymmetry and (1) we find the steady-state constraint

$$0 = \nabla\psi \cdot \boldsymbol{v}_E = (I/B^2)(\nabla\psi \times \nabla\varphi) \cdot (\nabla\phi). \tag{A.5}$$

Since both the axial and azimuthal derivatives of ϕ are zero, we find the steady-state constraint that $\phi = \phi(\psi)$ to leading order, as a consequence of perpendicular force balance.

For emphasis, this is only a constraint on the leading-order ϕ, of order $(\nabla\phi) \sim v_\mathrm{ti}B$. In the next section, we will evaluate a first-order (much smaller) potential $\phi_\sim$ that does vary within the flux surface.

[12] This equation neglects some small terms, particularly using $(\nabla p_s)/(Z_s e n_s \boldsymbol{u}_s \times \boldsymbol{B}) \sim (n_s T_s/\ell)/Z_s e n_s u_s B \sim (v_{\mathrm{t}s}/u_\varphi)[(v_{\mathrm{t}s}/\ell)/\Omega_s]$ and $[m_s n_s(\boldsymbol{u}_s \cdot \nabla)\boldsymbol{u}_s]/(Z_s e n_s \boldsymbol{u}_s \times \boldsymbol{B}) \sim (u_s/\ell)/\Omega_s \ll 1$.

Appendix A.3. Collisionless orbits ($v_{\mathrm{t}s}/\ell_z$)

Because $v_{\mathrm{t}s}/\ell_z \gg \nu_s$, particles typically complete many bounce orbits within a collision time, necessitating a kinetic treatment. At this frequency scale, each species' distribution function f_s (dependent on spatial position $\boldsymbol{x}$, velocity $\boldsymbol{v}$, and time t) evolves according to the Vlasov equation

$$\partial_t f_s + \boldsymbol{v} \cdot \nabla f_s + \frac{Z_s e}{m_s}(\boldsymbol{E} + \boldsymbol{v} \times \boldsymbol{B}) \cdot \partial_{\boldsymbol{v}} f_s = 0. \tag{A.6}$$

Consider first a steady state ($\partial_t \to 0$), and recall that when $\partial_t \phi = 0$ the collisionless particle orbits conserve the energy $H(\boldsymbol{x}, \boldsymbol{v}, t)$ from (3), meaning that[13]

$$\partial_t H + \boldsymbol{v} \cdot \nabla H + \frac{Z_s e}{m_s}(\boldsymbol{E} + \boldsymbol{v} \times \boldsymbol{B}) \cdot \partial_{\boldsymbol{v}} H = 0. \tag{A.7}$$

Still assuming $\partial_t \phi = 0$, any f_s that is a function of H alone will therefore be a steady-state solution of the Vlasov equation, since such an f_s evolves according to (A.7) times $(\partial_H f_s)$, by the chain rule. By the same logic, any f_s that is a function only of invariants of the collisionless motion (in our case, H, $\mathcal{P}_\varphi$, and μ) is a steady-state solution of the Vlasov equation. Any deviation from this dependence will cause variation at the $v_{\mathrm{t}s}/\ell_z$ frequency scale until f_s relaxes to $f_s(H, \mathcal{P}_\varphi, \mu)$.

To proceed, we generalize the approach of Sec. 2.2, recalling the approximate forms for H and $\mathcal{P}_\varphi$ from Eqs. (3) and (4). Treating the flux-function part of ϕ just as we did in Sec. 2.2, we now retain an additional weaker portion $\phi_\sim(\psi, z)$, which may vary within a flux surface. We can neglect the contribution of $\phi_\sim$ to $\boldsymbol{v}_E$, and may approximate $\phi_\sim(\psi, z) \approx \phi_\sim(\psi_0, z)$ in the small-gyroradius expansion. Eq. (8) then generalizes to

$$H - Z_s e\phi_0 \approx \frac{1}{2} m_s \tilde{v}_\parallel^2 - \frac{1}{2} m_s \omega_\varphi^2 R^2 + \mu B + Z_s e \phi_\sim. \tag{A.8}$$

For emphasis, the only change from (8) is the added term $Z_s e\phi_\sim$. In particular, ϕ_0 and ω_φ are evaluated with the leading-order zonal potential, $\tilde{v}_\parallel$ is exactly as defined in (10), and all functions are evaluated at $\psi = \psi_0$.

What does this mean for $\phi_\sim$? At our level of approximation, we may consider Eq. (A.8) at a fixed flux surface $\psi = \psi_0$, on which each species' distribution function is now a function of the invariants $f_s = f_s(H, \mathcal{P}_\varphi, \mu)$. Using the spatially varying Jacobian, $\int \mathrm{d}^3\boldsymbol{v} = (4\pi B/m_s^2) \int \mathrm{d}H \int \mathrm{d}\mu\, |\tilde{v}_\parallel|^{-1}$,[14] where $|\tilde{v}_\parallel|$ is a function of H, μ, and z via (A.8), we can calculate the

[13] In this formulation, $\boldsymbol{x}$, $\boldsymbol{v}$, and t are the independent variables, so e.g. $\boldsymbol{x}$ and t are held constant in the velocity partial $\partial_{\boldsymbol{v}}$. Note also that $\partial_{\boldsymbol{v}} v^2 = 2\boldsymbol{v}$.

[14] The given integral form assumes the integrand is even in $\tilde{v}_\parallel$, which is true for the integrals here. If the integrand is not even, one must use $\sum_{\sigma_v=+1,-1}(2\pi B/m_s^2) \int \mathrm{d}H \int \mathrm{d}\mu\, |\tilde{v}_\parallel|^{-1}$ where σ_v is the sign of $\tilde{v}_\parallel$.

z-dependent $n_s(z) = \int \mathrm{d}^3\boldsymbol{v}\, f_s(H, \mathcal{P}_\varphi, \mu)$.[15] Since the plasma is quasineutral to an excellent approximation (cf. Appendix A.5), it must satisfy

$$0 = \sum_s Z_s e n_s(z), \tag{A.9}$$

and this is the relationship that determines $\phi_\sim(z)$. Looking closer, the centrifugal potential $-\frac{1}{2}m_s\omega_\varphi^2 R^2$ acts to confine ions along the field, but is negligible for electrons. If we imagine that $\phi_\sim = 0$ at some time $t = 0$, then electrons would rapidly move outward in z at a rate $\sim v_{\mathrm{te}}/\ell_z$, and their outflux would drive the growth of an electron-confining $\phi_\sim(z)$ until their outflux was reduced to match that of the ions. [Since such a potential is de-confining for the ions, it will concurrently increase the ions' parallel outflux. However, it will not cancel the centrifugal confining force altogether, since $\phi_\sim$ only grows until the outflux of electrons and ions are equal.] Since electrons' kinetic energy is of order T_e, this implies a steady-state $\phi_\sim \sim T_\mathrm{e}/e$, much smaller than the leading-order flux-function potential. We will explicitly calculate a relevant special case of this relationship in Appendix A.4.

Appendix A.4. Collisional relaxation (ν_s)

Although the collisionless orbits allow an arbitrary dependence of the distribution functions f_s on the orbit invariants H, $\mathcal{P}_\varphi$, and μ, collisions relax the distribution function towards a Maxwellian $f_s \propto \exp(-H/T_s)$. However, any loss orbits are drained of particles at the collisionless transit rate $\sim v_{\mathrm{ts}}/\ell_z$, much faster than collisions can refill them. In this appendix, we will crudely treat this situation in a way that yields a more concrete estimate for the z-varying potential $\phi_\sim$.

Mechanically, the principal step here is to calculate the velocity-space boundaries for confined orbits, as a function of z over the confined-plasma region. For brevity, let's define a generalized species-dependent potential $\Phi_s \doteq Z_s e(\phi_0 + \phi_\sim) - \frac{1}{2}m_s\omega_\varphi^2 R^2$, so $H = \frac{1}{2}m_s\tilde{v}_\parallel^2 + \mu B + \Phi_s$. An orbit is confined if its orbit turns ($\tilde{v}_\parallel = 0$) for some z in the confinement region, equivalently if $H < \mu B_\mathrm{ec} + \Phi_{s,\mathrm{ec}}$. Conversely, an orbit only extends to those z for which $\tilde{v}_\parallel^2 > 0$, thus $H > \mu B + \Phi_s$, with $\mu > 0$ by definition. [We expect $\Phi_{s,\mathrm{ec}} \geq \Phi_s$ over the whole confined range of z, for both ions and electrons.[16]] With that, we will crudely take

$$f_s \approx c_{s0} e^{-H/T_s}\Theta(\mu B_\mathrm{ec} + \Phi_{s,\mathrm{ec}} - H)\Theta(H - \mu B - \Phi_s)\Theta(\mu), \tag{A.10}$$

with c_{s0} a normalizing constant and Θ the Heaviside function (equal to unity for positive argument, and to zero for negative argument). Of course, in a real system, collisions will distort f_s away from a Maxwellian for $(H, \mathcal{P}_\varphi, \mu)$ near to the loss boundary, but in a well-confined centrifugal system this distortion should be weak outside a relatively small fraction of phase space, motivating our *ad hoc* approximation.

One can straightforwardly (if tediously) evaluate the velocity-space integral to obtain[17]

$$\frac{e^{\Phi_s/T_s}}{(2\pi)^{3/2}v_{\mathrm{ts}}^3 c_{s0}} n_s = 1 - \mathrm{erfc}(\Phi_{s\Delta}^{1/2}) \cdots + B_\Delta^{1/2} e^{\Phi_{s\Delta}(1-B_\Delta)/B_\Delta}\mathrm{erfc}(\sqrt{\Phi_{s\Delta}/B_\Delta}), \tag{A.11}$$

with normalized nonnegative functions $\Phi_{s\Delta} \doteq (\Phi_{s,\mathrm{ec}} - \Phi_s)/T_s$ and $B_\Delta \doteq (1 - B/B_\mathrm{ec})$, and with erfc the complementary error function. Physically, the "1" on the RHS captures the basic Gibbs (adiabatic) response to Φ_s,[18] and the two erfc terms capture the μ-dependent loss cone. Approaching the boundary points, where both $\Phi_{s\Delta}$ and B_Δ go to zero, the last term of (A.11) goes to zero[19] and the second-last term approaches (-1), correctly indicating that the confined-plasma density goes to zero there.[20] In a deeply-confined plasma away from the endcap/loss points, $\Phi_{s\Delta}$ becomes large-ish (comparable to M_i^2) but $B_\Delta < 1$, and the erfc corrections become very small. See Fig. A1.

[15] It may appear somewhat mysterious that the spatial dependence enters through the Jacobian in $\mathrm{d}^3\boldsymbol{v}$. This happens because the Vlasov equation's characteristics (single-particle trajectories) are divergence-free in the 6-dimensional $(\boldsymbol{x}, \boldsymbol{v})$ phase space, but the trajectories are not divergence-free in $\boldsymbol{x}$-space alone.

[16] On one hand, this seems trivial—the centrifugal force confines ions, and $\phi_\sim$ confines electrons. However, the centrifugal confinement is in fact also electrostatic, as we discussed in Sec. 2.4. The key here is that the ions, with their greater mass, undergo a much wider radial drift orbit, which leads to electrostatic confinement by drift motion up or down the radial gradient of the leading-order flux-function potential, overpowering the smaller deconfining-for-ions force from $\partial_z\phi_\sim$.

[17] First carry out the μ integral, with the velocity-space Jacobian from Appendix A.3 and $|\tilde{v}_\parallel| = [2(H - \mu B - \Phi_s)/m_s]^{1/2}$, obtaining

$$\frac{m_s^{3/2}}{2^{5/2}\pi c_{s0}} n_s = \frac{m_s^{3/2}}{2^{5/2}\pi c_{s0}} \int \mathrm{d}^3\boldsymbol{v}\, f_s = \int_{\Phi_s}^{\Phi_{s,\mathrm{ec}}} \mathrm{d}H\, e^{-H/T_s}\,(H - \Phi_s)^{1/2} + \int_{\Phi_{s,\mathrm{ec}}}^{\infty} \mathrm{d}H\, e^{-H/T_s}[H(1 - B/B_\mathrm{ec}) + \Phi_{s,\mathrm{ec}}B/B_\mathrm{ec} - \Phi_s]^{1/2}.$$

For the two H integrals, change the integration variables to $t \doteq [(H - \Phi_s)/T_s]^{1/2}$ and $t \doteq [(H + b)/T_s]^{1/2}$, with constant $b \doteq (\Phi_{s,\mathrm{ec}}B/B_\mathrm{ec} - \Phi_s)/(1 - B/B_\mathrm{ec})$. Integrate the results by parts using $\partial_t e^{-t^2} = -2te^{-t^2}$ and note that the boundary terms cancel.

[18] Interestingly, the Gibbs response also retains effects of the mirror force, even though neither μ nor B appear explicitly. In essence, the volume element is smaller where B is larger, due to $\nabla \cdot \boldsymbol{B} = 0$, so it contains less particles even at the same density.

[19] Note that $0 \leq e^{\Phi_{s\Delta}/B_\Delta}\mathrm{erfc}(\sqrt{\Phi_{s\Delta}/B_\Delta}) \leq 1$, for all positive $(\Phi_{s\Delta}/B_\Delta)$.

[20] There will be a very small outflowing plasma density on the loss orbits, but that is not included in this density estimate.

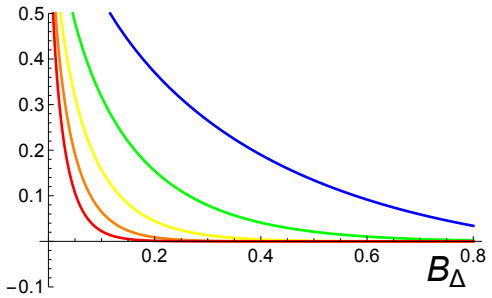

Figure A1. Plots of $(1 - n_s e^{\Phi_s/T_s}/2^{3/2}\pi^{3/2}v_{ts}^3 c_{s0})$ as a function of B_Δ for $\Phi_{s\Delta}/B_\Delta$ (moving downwards) of 1, 4, 9, 16, and 25. As these lines approach zero, n_s approaches a Gibbs response. All lines go to unity as $B_\Delta \to 0$, meaning that no confined orbits remain at the actual throat of the endcap, where $B = B_{\rm ec}$ and $\Phi_s = \Phi_{s,{\rm ec}}$.

We can use Eq. (A.11) to more concretely evaluate the quasineutrality relation (A.9). For simplicitly, consider a well-confined case, where $(\Phi_{s,{\rm ec}} - \Phi_s)/T_s$ is rather larger than one (although still order unity) in the bulk/central column. Focusing on this central region, the erfc terms of (A.11) may be neglected relative to the Gibbs response. Defining constant $n_{s0} \doteq (2\pi)^{3/2} v_{ts}^3 c_{s0} e^{-\Phi_s(z=0)/T_s}$ and function $\tilde\Phi_s(z) \doteq \Phi_s(z) - \Phi_s(z=0)$, we may replace the first term of (A.11) with $n_s(z)/(n_{s0}e^{-\tilde\Phi_s/T_s})$ so, when the erfc terms are negligible,

$$n_s(z) \approx n_{s0} e^{-\tilde\Phi_s(z)/T_s}. \tag{A.12}$$

Letting $\tilde\phi_\sim(z) \doteq \phi_\sim(z) - \phi_\sim(z=0)$ and $R_0 \doteq R(z=0)$ here,[21] we have $\tilde\Phi_s(z) = Z_s e\tilde\phi_\sim + \frac{1}{2}m_s\omega_\varphi^2(R_0^2 - R^2)$, with $\tilde\Phi_{\rm e} \approx -e\tilde\phi_\sim$ for the electrons. With $\sum_{s\in{\rm i}}$ indicating a sum over only ionic species (i.e. excluding electrons), we can rewrite (A.9) here as

$$n_{\rm e0} e^{e\tilde\phi_\sim/T_{\rm e}} \approx \sum_{s\in{\rm i}} Z_s n_{s0} e^{-Z_s e\tilde\phi_\sim/T_s - \frac{1}{2}m_s\omega_\varphi^2(R_0^2-R^2)/T_s}, \tag{A.13}$$

with the special case $n_{\rm e0} = \sum_{s\in{\rm i}} Z_s n_{s0}$ at $z = 0$. At any fixed $z \neq 0$, the LHS increases monotonically with $\tilde\phi_\sim$ while the RHS decreases monotonically, so we expect they will be equal at a single, unique value of $\tilde\phi_\sim(z)$, making the problem well posed.

For physical understanding, we consider the special case of a single ionic species. In this case $n_{\rm e0} = Z_{\rm i} n_{\rm i0}$ and we can rearrange (A.13) to

$$e^{e\tilde\phi_\sim(Z_{\rm i}T_{\rm e}+T_{\rm i})/T_{\rm i}T_{\rm e}} \approx e^{-\frac{1}{2}m_{\rm i}\omega_\varphi^2(R_0^2-R^2)/T_{\rm i}} \tag{A.14}$$

thus

$$e\tilde\phi_\sim/T_{\rm e} \approx -\frac{1}{2}m_{\rm i}\omega_\varphi^2(R_0^2 - R^2)/(Z_{\rm i}T_{\rm e} + T_{\rm i}). \tag{A.15}$$

As expected, $\tilde\phi_\sim$ is negative and of order $T_{\rm e}/e$, forming a potential barrier for the electrons and weakening (but not eliminating) the ion potential barrier, leading to ambipolar parallel confinement:

$$\tilde\Phi_{\rm e}/T_{\rm e} = \tilde\Phi_{\rm i}/T_{\rm i} = \frac{1}{2}m_{\rm i}\omega_\varphi^2(R_0^2 - R^2)/(Z_{\rm i}T_{\rm e} + T_{\rm i}). \tag{A.16}$$

In this special case, the solution for $\phi_\sim$ from (A.15) holds unmodified even where the erfc terms become nonnegligible, since (A.16) also implies $\Phi_{{\rm e}\Delta} = \Phi_{{\rm i}\Delta}$. In the cold-electron limit $Z_{\rm i}T_{\rm e} \ll T_{\rm i}$, the $\phi_\sim$ necessary to confine the electrons is negligible in the ion dynamics, in which case the treatment in Sec. 2 (focusing on ion force balance and neglecting $\phi_\sim$ altogether) is quantitatively justified.

We conclude that the plasma develops a potential $\phi_\sim$ that varies in a flux surface but is much smaller than the leading-order flux-function ϕ, and that this potential $\phi_\sim$ ensures that quasineutrality is maintained along the entirety of the confined plasma. This is maintained by dynamics local to the confined-plasma region, and does not depend on specific assumptions about the endcap regions.

Appendix A.5. Momentum transport and axial current ($\tau_{\rm c}^{-1}$)

We have seen that the leading-order potential is a flux function (Appendix A.2) that it is roughly unaffected by electron parallel dynamics, which are restricted to an ambipolar level by the much-smaller $\phi_\sim$ (Appendix A.3 and Appendix A.4). In this appendix, we see how the leading-order potential evolves in time, on the slowest $\tau_{\rm c}^{-1}$ frequency scale, controlled by the transport of conserved angular momentum.

Our system conserves angular momentum because the single-particle orbits conserve canonical angular momentum $\mathcal{P}_\varphi$, defined in (4), fundamentally due to azimuthal symmetry. Considering $\mathcal{P}_\varphi = \mathcal{P}_\varphi(\boldsymbol{x}, \boldsymbol{v})$ for an axisymmetric, time-independent magnetic field, one may show the $\mathcal{P}_\varphi$ analog to (A.7):[22]

$$d_t\mathcal{P}_\varphi \doteq \partial_t\mathcal{P}_\varphi + \boldsymbol{v}\cdot\nabla\mathcal{P}_\varphi + \frac{Z_s e}{m_s}(\boldsymbol{E} + \boldsymbol{v}\times\boldsymbol{B})\cdot\partial_{\boldsymbol{v}}\mathcal{P}_\varphi = 0. \tag{A.17}$$

Although the electromagnetic part of $\mathcal{P}_\varphi$ is the larger part for any single particle, $m_s R v_\varphi/Z_s e\psi \sim \rho_{\varphi,z}/R$,[23] its contribution to the total momentum balance is constrained by quasineutrality: Consider a volume V bounded radially by a constant-ψ surface S_ψ, and axially by two axisymmetric surfaces S_{z_+} and S_{z_-}, which are aligned with $\nabla\psi$ and lay within the z range

[21] Note that this is a distinct usage from the R_0 in Table (A1).

[22] Note that $Rv_\varphi = R\hat{\boldsymbol{\varphi}}\cdot\boldsymbol{v}$, in which $R\hat{\boldsymbol{\varphi}} = \hat{\boldsymbol{z}}\times\boldsymbol{x}$ depends only on $\boldsymbol{x}$. Recalling that ∇ is taken at fixed $\boldsymbol{v}$, one finds (e.g. using Cartesian components) that $\nabla(Rv_\varphi) = -\hat{\boldsymbol{z}}\times\boldsymbol{v}$, so $\boldsymbol{v}\cdot\nabla(Rv_\varphi) = 0$. Also, since $\partial_{\boldsymbol{v}}(Rv_\varphi) = R\hat{\boldsymbol{\varphi}}$, we have $\boldsymbol{E}\cdot\partial_{\boldsymbol{v}}(Rv_\varphi) = 0$ by axisymmetry, and [recalling (1)] $(\boldsymbol{v}\times\boldsymbol{B})\cdot\partial_{\boldsymbol{v}}(Rv_\varphi) = \boldsymbol{v}\cdot\boldsymbol{B}\times R\hat{\boldsymbol{\varphi}} = -\boldsymbol{v}\cdot\nabla\psi$

[23] Recall (2).

of confined particle orbits.[24] Charge conservation ($\partial_t \rho_{\rm ch} = -\nabla\cdot\boldsymbol{j}$) and Gauss's Law, integrated over this volume, give us

$$\epsilon_0\partial_t\Big[\int_{S_\psi}\mathrm{d}\boldsymbol{S}\cdot\boldsymbol{E}+\sum_{z_+,z_-}\int\mathrm{d}\boldsymbol{S}\cdot\boldsymbol{E}\Big] = -\int_{S_\psi}\mathrm{d}\boldsymbol{S}\cdot\boldsymbol{j}-\sum_{z_+,z_-}\int\mathrm{d}\boldsymbol{S}\cdot\boldsymbol{j} \quad (A.18)$$

Since the endcap surfaces have $\mathrm{d}\boldsymbol{S}\perp\nabla\psi$, the term $\sum_{z_+,z_-}\int\mathrm{d}\boldsymbol{S}\cdot\boldsymbol{E} = -\sum_{z_+,z_-}\int\mathrm{d}\boldsymbol{S}\cdot\nabla\phi_\sim$ may be neglected relative to $\int_{S_\psi}\mathrm{d}\boldsymbol{S}\cdot\boldsymbol{E}\approx-\int_{S_\psi}\mathrm{d}\boldsymbol{S}\cdot\omega_\varphi\nabla\psi$. For S_ψ, some geometry: First, since S_ψ is a surface of constant ψ, its normal is parallel to $\nabla\psi$, so one has $\mathrm{d}\boldsymbol{S} = \sigma_\psi\,\mathrm{d}S(\nabla\psi)/|\nabla\psi|$, with $\sigma_\psi=\pm1$ the sign of $\partial_R\psi$. Second, since two nearby flux surfaces ψ and $\psi+\mathrm{d}\psi$ are spaced physically by $\mathrm{d}\psi/|\nabla\psi|$, the volume element at S_ψ may be written as $\mathrm{d}^3\boldsymbol{x} = \mathrm{d}S\,\mathrm{d}\psi\,|\nabla\psi|^{-1}$ and the total volume between the adjacent surfaces is $V'\mathrm{d}\psi$ for flux function $V'\doteq\int_{S_\psi}\mathrm{d}S\,/|\nabla\psi|$. The flux-surface average $\langle\cdots\rangle$, defined as the volume average taken at a flux surface, may be written for S_ψ as $\langle\cdots\rangle = (V')^{-1}\int_{S_\psi}\mathrm{d}S\,|\nabla\psi|^{-1}$. With that, and recalling (1), we can relate the first term in (A.18) to the field (Poynting) angular momentum since

$$-\langle\epsilon_0\boldsymbol{E}\times\boldsymbol{B}\cdot R\hat{\boldsymbol{\varphi}}\rangle = \langle\epsilon_0\boldsymbol{E}\cdot\nabla\psi\rangle = \frac{\sigma_\psi}{V'}\epsilon_0\int_{S_\psi}\mathrm{d}\boldsymbol{S}\cdot\boldsymbol{E}. \quad (A.19)$$

Assuming that S_ψ is chosen inside the confined-plasma volume, we may evaluate $\boldsymbol{j} = \sum_s\int\mathrm{d}^3\boldsymbol{v}\,Z_s e f_s\boldsymbol{v}$, so

$$\frac{1}{V'}\int_{S_\psi}\mathrm{d}\boldsymbol{S}\cdot\boldsymbol{j} = \sigma_\psi\langle\boldsymbol{j}\cdot\nabla\psi\rangle = \sigma_\psi\sum_s\Big\langle\int\mathrm{d}^3\boldsymbol{v}\,f_s d_t(Z_s e\psi)\Big\rangle. \quad (A.20)$$

For the mechanical angular momentum, we act on Eq. (A.6) with $\sum_s\int\mathrm{d}^3\boldsymbol{v}\,m_sRv_\varphi$, doing some integrations by parts to find[25]

$$\partial_t\sum_s\int\mathrm{d}^3\boldsymbol{v}\,m_sRv_\varphi f_s+\nabla\cdot\Big[\sum_s\int\mathrm{d}^3\boldsymbol{v}\,m_sRv_\varphi\boldsymbol{v}f_s\Big] = \sum_s\int\mathrm{d}^3\boldsymbol{v}\,f_s d_t(m_sRv_\varphi), \quad (A.21)$$

which we will flux-surface average. Using (A.17) to replace $d_t(m_sRv_\varphi) = -d_t(Z_se\psi)$ in the last term, we may equate

$$V'\Big\langle\sum_s\int\mathrm{d}^3\boldsymbol{v}\,f_s d_t(m_sRv_\varphi)\Big\rangle = -\sigma_\psi\int_{S_\psi}\mathrm{d}\boldsymbol{S}\cdot\boldsymbol{j}$$
$$\approx -V'\partial_t\langle\epsilon_0\boldsymbol{E}\times\boldsymbol{B}\cdot R\hat{\boldsymbol{\varphi}}\rangle+\sigma_\psi\sum_{z_+,z_-}\int\mathrm{d}\boldsymbol{S}\cdot\boldsymbol{j}. \quad (A.22)$$

The field momentum term is much smaller than the $\boldsymbol{E}\times\boldsymbol{B}$ contribution to the physical momentum term $\partial_t\sum_s\int\mathrm{d}^3\boldsymbol{v}\,m_sRv_\varphi f_s$, since[26]

$$\frac{\epsilon_0\boldsymbol{E}\times\boldsymbol{B}\cdot R\hat{\boldsymbol{\varphi}}}{\sum_s\int\mathrm{d}^3\boldsymbol{v}\,m_sRv_{E\varphi}f_s} = \frac{\epsilon_0\boldsymbol{E}\times\boldsymbol{B}\cdot R\hat{\boldsymbol{\varphi}}}{\rho_{\rm m}\boldsymbol{E}\times\boldsymbol{B}\cdot R\hat{\boldsymbol{\varphi}}/B^2} = \frac{v_{\rm A}^2}{c^2}\ll1. \quad (A.23)$$

For Table A1 parameters, $v_{\rm A}^2/c^2\approx2.4\cdot10^{-4}$. This is one statement of quasineutrality—it implies that we may neglect the $\propto\partial_t\boldsymbol{E}$ terms relative to the $\propto\boldsymbol{j}$ terms in (A.18). Physically, a changing electric field corresponds to a changing $\boldsymbol{E}\times\boldsymbol{B}$ angular momentum, and ions move radially as they pick up this azimuthal momentum, similar to the newly-ionized ion in Sec. 2.3. The ion charge density resulting from this radial shift is much larger than the actual net charge density.

With that, our flux-surface averaged angular momentum equation is[27]

$$\sum_s\Big[\partial_t\langle\int\mathrm{d}^3\boldsymbol{v}\,m_sRv_\varphi f_s\rangle+\frac{1}{V'}\partial_\psi\langle V'\int\mathrm{d}^3\boldsymbol{v}\,m_sRv_\varphi f_s\boldsymbol{v}\cdot\nabla\psi\rangle\Big]$$
$$\approx\sum_{z_+,z_-}\Big[\frac{-2\pi R\sigma_\pm}{V'|\nabla\psi|}\sum_s\int\mathrm{d}^3\boldsymbol{v}\,m_sRv_\varphi f_s\boldsymbol{v}\cdot\hat{\boldsymbol{b}}_{\rm ax}+\frac{\sigma_\psi}{V'}\int\mathrm{d}\boldsymbol{S}\,j_\psi\Big] \quad (A.24)$$

with unit vector $\hat{\boldsymbol{b}}_{\rm ax}\doteq(\nabla\psi\times\nabla\varphi)/|\nabla\psi\times\nabla\varphi|$, and $\sigma_\pm=\pm1$ chosen at each end (z_+, z_-) so $\sigma_\pm\hat{\boldsymbol{b}}_{\rm ax}$ points outward towards the endcaps. Physically, the flux-surface-averaged angular momentum (first term) evolves in time due to outfluxes of mechanical angular momentum in the radial (second term) and axial (third term) directions, and due to a net outgoing axial current (fourth term, equal and opposite to net incoming radial current by quasineutrality). For the end fluxes (second row), note that only the mechanical momentum outflux at the surface ψ contributes, while the entire outgoing current (axis to the ψ surface) contributes to the final term.

Although a comprehensive transport analysis is beyond the scope of this article, we briefly consider the terms in the momentum transport equation (A.24), focusing on the ways that they are constrained by the steady states of the more rapid timescales. Let's start with radial transport, the second term of (A.24). At the most rapid rates $\sim\Omega_s$, the radial flow $\boldsymbol{v}\cdot\nabla\psi$ is blocked by gyro-motion and the fact that ϕ is a flux function to leading order, so $\boldsymbol{v}_E\cdot\nabla\psi=0$. At the next-slower rate $\sim v_{{\rm t}s}/\ell$, recall that the collisionless orbits followed surfaces of constant H, $\mathcal{P}_\varphi$, and μ,

[24] The axial-bounding surfaces S_{z+} and S_{z-} are close to constant-z discs, but are a bit bent in the z direction so that they are normal to the flux surfaces, thus have $\mathrm{d}\boldsymbol{S}\perp\nabla\psi$.

[25] At this slow frequency scale, we should retain the collision operator in (A.6). However, collisions conserve momentum, so that contribution sums to zero here.

[26] Use $v_{E\varphi} = (\boldsymbol{E}\times\boldsymbol{B}\cdot\hat{\boldsymbol{\varphi}})/B^2$, $\sum_s\int\mathrm{d}^3\boldsymbol{v}\,m_sf_s=\rho_{\rm m}$, and $\epsilon_0\mu_0=1/c^2$.

[27] To evaluate the flux-surface average of the flux-divergence term (2nd on LHS), it may be easiest to evaluate the flux-surface average as a derivative of the volume average over V, that is, $\langle\cdots\rangle=\sigma_\psi(V')^{-1}\partial_\psi\int_V\mathrm{d}^3\boldsymbol{x}$. Before differentiating in ψ, use the divergence theorem on the volume integral. The surface integral at the endcaps may be explicitly written as $\sum_{z_+,z_-}\int\mathrm{d}\boldsymbol{S}=\sum_{z_+,z_-}2\pi\sigma_\pm\int_0^\psi\mathrm{d}\psi'\,R|\nabla\psi|^{-1}\hat{\boldsymbol{b}}_{\rm ax}$.

which causes their poloidal projection to be closed, so their $\boldsymbol{v}\cdot\nabla\psi$ averages to zero. Collisions allow particles to take radial steps, of width the gyro-orbit ($\sim \rho_s = v_{ts}m_s/Z_seB$) for $B_\varphi = 0$ (causing classical transport) or of width the drift orbit ($\sim \rho_{s,z} \doteq v_{ts}m_s/Z_seB_z$) for $B_\varphi \neq 0$. In either case, there is a radial diffusivity ($\sim \nu_s\rho_s^2$ or $\sim \nu_s\rho_{sz}^2$, respectively), and in either case the transport is ambipolar (because collisions conserve total momentum, and the radial step is proportional to the change in momentum).[28] This drives radial transport at a rate $\sim \nu_s\rho_s^2/\ell^2$ or $\nu_s\rho_{s,z}^2/\ell^2$, in either case much slower than ν_s. It cannot directly drive radial current, since the transport is intrinsically ambipolar. There may also be turbulent transport, although this is potentially weakened by the strong $\boldsymbol{E}\times\boldsymbol{B}$ shear in the centrifugal mirror.

Consider next the parallel mechanical momentum end loss, the third term of (A.24). This case is again constrained by the fact that the collisionless orbits are closed, within the confined plasma region. Again, collisions can scatter particles onto loss orbits, but this process is slowed by the strong centrifugal potential barrier for ions and comparably strong electrostatic barrier for electrons, the $\Phi_{s,\mathrm{ec}}$ from Appendix A.4, so only $\sim \exp(-\Phi_s/T_s)$ particles have enough energy to escape, with $\Phi_s/T_s \sim M_\mathrm{i}^2$. As discussed e.g. by EHMO, this leads to a parallel loss rate of order $\nu_s(4/M_\mathrm{i}^2)\exp(-M_\mathrm{i}^2/4) \ll \nu_s$. Since the momentum is mostly carried by ions, the momentum end losses may only occur at their slower rates, evaluated with ν_i. The example τ_c^{-1} from Appendix A.1 is at the faster electron rate and captures a parallel heat-loss channel.

Consider now the current end losses, the fourth term of (A.24). Note first that this integral goes radially from the reference flux surface all the way in to the axis of symmetry, so it includes not only plasma current, but also any net current entering or leaving the (solid) central conductor (at the trap's axis of symmetry, $R = 0$). Indeed, this central-conductor current supplies the torque to drive the plasma rotation, but it will generally relax to ∼transport rates in any steady state, since the conductor is usually held at a fixed, time-independent potential. Consider then the plasma portion of $\sum_{z_+,z_-}\int \mathrm{d}\boldsymbol{S}\cdot\boldsymbol{j}$. Of course, with insulating endcaps, one should strictly set this to zero, but perhaps the endcap region or end insulator is leaky somehow and permits some outgoing current. Even in this case, the upstream balances will restrict outgoing current. The closed collisionless orbits independently restrict individual species' outgoing fluxes thus also current, but the constraint on $\boldsymbol{j}$ is even stricter. As we saw in Appendix A.3 and Appendix A.4, the confined-plasma region fluxes relax the potential $\phi_\sim$ so that parallel fluxes are ambipolar, and this requires only a $\phi_\sim$ that is much smaller than the leading-order flux-function potential. Given this, and assuming a well-confined centrifugal mirror, even with leaky endcap regions the outgoing current would be restricted to the rate at which transport can supply cross-field radial current divergence, which must then be balanced by outgoing current to restore the ambipolar $\phi_\sim$. Since that upstream charge density mostly results from ion radial drifts due to momentum transport, that limits the outgoing current term to be of a similar magnitude, even if the endcaps were to tolerate $\int \mathrm{d}\boldsymbol{S}\cdot\boldsymbol{j} \neq 0$.

[28] In detail, for neoclassical transport: The collisionless orbits conserve $\mathcal{P}_\varphi$, which determine's a particle's radial position (start of Sec. 2.2). A collision transfers momentum between two particles, conserving the sum. This occurs at fixed ψ, thus changes their $\mathcal{P}_\varphi$, thus their radial orbit center $\approx \psi_0 = \mathcal{P}_\varphi/Z_se$. Recalling (4), the equal and opposite increments to $\mathcal{P}_\varphi$ correspond to equal and opposite steps of $Z_se\psi_0$, thus zero radial current.

Appendix B. Endcap current to relax MHD constraints

In Sec. 3, we found that the MHD equilibrium beta limits were set by axial magnetic field ($\approx B_z$) alone. For a beta-limited plasma, this means that the addition of B_φ does not permit any reduction of B_z, and therefore also no reduction of the applied voltage. For example, B_φ could not meaningfully reduce the voltage required for EHMO's reactor design point (see Appendix A.1). But could we get around this restriction if we were somehow able to allow some current out the endcaps? What would the requirements be? In this appendix, we offer brief analysis of these questions.

To evaluate this, we revisit Sec. 3 but relax the analysis to allow current out the ends. The analysis in Sec. 3.1 proceeds completely unchanged—those conclusions rested only on force balance within the plasma, leading-order particle confinement, and Ampère's Law.[29] In particular, even if we allow outgoing current, the equilibrium must still satisfy (36) [equivalently (37)] with $I = I(\psi)$ [due to (34)]. However, a nonzero outgoing current would allow $I' \neq 0$, cf. (40) and adjacent discussion.

How big would this current need to be in order to effectively relax the MHD beta constraints? To get the basic magnitude, let's estimate the axial current-density j_ax that we would need in order to do the entire radial force balance, for example by solving (36) with

[29] Note that no matter how you drive the plasma currents, within the plasma volume they must still be consistent with force balance and with Ampère's Law.

$(\Delta^*\psi)$ set to zero.[30] Unwinding our definitions,[31] we find (neglecting $\partial_\psi p$ relative to the larger centrifugal term)

$$j_{\rm ax} \sim \rho_{\rm m}\omega_\varphi^2 R/B_\varphi, \tag{B.1}$$

simply the axial current for which $\boldsymbol{j}\times B_\varphi\hat{\boldsymbol{\varphi}}$ balances the outward centrifugal force.

As one possibility, suppose we generated this current purely through plasma losses, somehow letting all ions escape axially in one direction and electrons in the other. The corresponding density outflux would limit the density confinement rate to

$$\tau_n^{-1} \sim n_{\rm e}^{-1} j_{\rm ax}/e\ell_z \sim (\omega_\varphi/\Omega_{\rm i})(u_\varphi/\ell_z), \tag{B.2}$$

only one order smaller than simple thermal outflows. This is much too rapid for a reactor. For example, for the parameters from Table A1 this is around $\tau_n \sim 1.8\cdot 10^3{\rm s}^{-1}$, much more rapid than their estimated $\tau_{\rm c}$.

As another possibility, suppose we somehow emitted a current from one end insulator and let it pass through the plasma, absorbing it into the other. An electron current would be most practical, because the light electrons carry more current per heat flux, and they would not contribute to the outward centrifugal force in the bulk plasma region. They would be accelerated into the plasma by $\phi_\sim$, passing through the confined-plasma region with a kinetic energy around $M_{\rm i}^2 T_{\rm e}$ [cf. (A.15)] thus speed around $M_{\rm i} v_{\rm te}$ and correspondingly low collisionality. They would be decelerated again by $\phi_\sim$ on the way out to the far endcap. However, the currents required are almost certain to be impractically large. For Table A1 parameters, taking B_φ =2.6T, the current density from (B.1) times a cross-sectional plasma area around $2\pi R_0(\Delta R)$ comes to an axial current of around 10^7A.

References

[1] Lehnert B 1971 *Nucl. Fusion* **11** 485–533

[2] Baker D A, Hammel J E and Ribe F L 1961 *Phys. Fluids* **4** 1534–1548

[3] Ellis R F, Hassam A B, Messer S and Osborn B R 2001 *Phys. Plasmas* **8** 2057–2065

[4] Hassam A B 1997 *Comments Plasma Phys. Controlled Fusion* **18** 263–279

[5] Teodorescu C *et al.* 2010 *Phys. Rev. Lett.* **105** 085003

[30] This balance does not work in detail, because $I'I$ is a flux function, but the pressure and centrifugal terms are not. However, we can still estimate the current density $j_{\rm ax}$ that would be needed for I' to provide a significant fraction of the radial confinement.

[31] Eq. (40) gives $\mu_0 j_{\rm ax} = I'|\nabla\psi|/R$, Eq. (36) with $(\Delta^*\psi)\to 0$ gives us I', Eq. (2) gives us $\partial_\psi R \sim (1/\partial_R\psi) = 1/RB_z \sim 1/|\nabla\psi|$, and (1) relates I, $\nabla\psi$, and components of $\boldsymbol{B}$.

[6] Hassam A B 1992 *Phys. Fluids B* **4** 485–487

[7] Huang Y M and Hassam A B 2001 *Phys. Rev. Lett.* **87** 235002

[8] Messer S, Ellis R, Case A, Gupta D, Hassam A, Lunsford R and Teodorescu C 2005 *Phys. Plasmas* **12** 062509

[9] White R, Hassam A and Brizard A 2018 *Phys. Plasmas* **25** 012514

[10] Teodorescu C, Clary R, Ellis R F, Hassam A B, Lunsford R, Uzun-Kaymak I and Young W C 2008 *Phys. Plasmas* **15** 042504

[11] Burdakov A V, Ivanov A A and Kruglyakov E P 2010 Progress in studies of magnetic mirrors and their prospects presented at the IAEA FEC

[12] Belova E V, Gorelenkov N N and Cheng C Z 2003 *Phys. Plasmas* **10** 3240–3251

[13] Romero-Talamás C A, Elton R C, Young W C, Reid R, Ellis R F and Hassam A B 2010 *Journal of Fusion Energy* **29** 543–547

[14] Hazeltine R D and Waelbroeck F L 2004 *The Framework of Plasma Physics* (Boulder, CO: Westview Press)

[15] Pastukhov V P 1974 *Nucl. Fusion* **14** 3–6

[16] Helander P and Sigmar D J 2002 *Collisional Transport in Magnetized Plasmas* (Cambridge UP)

[17] Freidberg J P 2014 *Ideal MHD* (Cambridge UP)

[18] Valanju P M, Mahajan S M and Quevedo H J 2006 *Phys. Plasmas* **13** 062105